

On the usage of Flaring Gas Layers to determine the Shape of Dark Matter Halos

To appear in the August 1995 issue of *The Astronomical Journal*

Rob P. Olling
Columbia University

ABSTRACT

I present a new method of deriving the shape of the dark matter (DM) halos of spiral galaxies. The method relies on the comparison of model predictions with high spectral and spatial resolution HI observations of the gas layer. So far, determinations of the flaring of the gas layer (i.e. the increase of the thickness with galactocentric radius) have been used to determine the mass-to-light ratio, \mathcal{M}/\mathcal{L} , of the stellar disk of several edge-on galaxies. In this paper I describe a method which can be used to determine the shape of DM-halos. This technique will be applied in a forthcoming paper.

I show that the model predictions of the gas layer width are best calculated using a global approach, in which the potential arising from the *total* mass distribution of the galaxy is used in the calculation of the vertical distribution of the gas. I developed a new algorithm to calculate the force field of an arbitrary, azimuthally symmetric, density distribution. This algorithm is used to calculate the forces due to the radially truncated stellar disk as well as of the flaring gas layer.

I use a simple two-parameter family of disk-halo models which have essentially the same observed equatorial rotation curve but different vertical forces. This mass model is composed of a stellar disk with constant \mathcal{M}/\mathcal{L} , and a DM-halo with a given axial ratio (Sackett & Sparke [ApJ, 1990, 361, 408]). I approximate the radial force due to the gaseous disk, and iteratively determine the vertical force due to the global distribution of the gas.

In agreement with Maloney [ApJ, 414, 41, 1993] I find that beyond the Holmberg radius, the thickness of the gaseous disk is sensitive to both the flattening of the DM-halo and the self-gravity of the gas. I also show that the inferred DM-halo flattening is not sensitive to the particular choice of disk-halo decomposition.

I show that the determination of the thickness of the gas layer is not restricted to edge-on galaxies, but can be measured for moderately inclined systems as well. Thus, in combination with detailed modeling, high resolution HI imaging of nearby galaxies with extended HI envelopes will enable us to determine the shape of the DM halo of these galaxies.

1. Introduction

Until recently, little was known about the shape of dark halos : measurements of the equatorial rotation curve provide a one dimensional probe to the potential only. It is possible to construct both spherical and flat mass models which generate the same rotation curve. Therefore, the shape of the dark halo can not be inferred from galactic rotation curves alone.

Existing methods to estimate the shape of DM-halos have given mixed results. It has been suggested (Dekel & Shlosman, 1983; Toomre, 1983; Sparke & Casertano, 1988) that galactic warps, frequently observed in the outer parts of gaseous disks, result if the galactic disk is tilted with respect to the plane of a flattened dark halo. Hoffner & Sparke (1994) investigated the time evolution of such warps and concluded that only one out of the five systems they studied requires a halo as flattened as E6. Polar ring galaxies, early type spirals with material rings in a plane perpendicular to the galaxy plane, probe the dark halo potential in two perpendicular directions. Careful analysis of the stellar and gas dynamics of the polar ring system NGC 4650A, led Sackett & Sparke (1990, hereafter SS90) and Sackett *et al.* (1994, SRJF94 hereafter) to conclude that the dark halo in this system could be as flattened as E6-E7 ($q=0.4$ to 0.3). Recently, Sackett *et al.* (1994b) reported the discovery of a rather flattened ($q \approx 0.5$) *luminous* halo around the edge-on spiral NGC 5907, which can account for the observed rotation curve provided that this luminous material has a large mass-to-light ratio (≈ 450).

Like the polar rotation curve, the thickness of the gas layer depends on the vertical force, K_z , and hence on the shape of the DM-halo (Maloney 1992; Olling & van Gorkom 1992; Kundić *et al.* 1993, KHG93; Maloney 1993, M93). That the shape of the dark halo influences the vertical distribution of the gas can be easily understood. Consider a round halo, with a certain density distribution, then decrease the vertical scale-height while maintaining the total mass. Consequently, the densities as well as the exerted gravitational forces will increase, resulting in a thinner HI disk and higher rotation speeds. In order to keep the same equatorial rotation curve, one has to deform the DM-halo in a very specific way (Appendix A, Figure 2) as a result of which the DM-halo densities (at large distances) will be roughly inversely proportional to the flattening q ($= c/a$). In accordance

with Maloney (1993), I find that (at large distances) the thickness of the gas layer is roughly proportional to the square root of the halo flattening, q . Several authors have employed measurements of the gas layer thickness to infer the total mass density in the plane of spiral galaxies. Van der Kruit (1981) showed that the width of a galaxy's gaseous disk should increase radially in an exponential fashion. From the thickness measurements of the gaseous disk of the edge-on galaxy NGC 891 by Sancisi & Allen (1979) van der Kruit concluded that the \mathcal{M}/\mathcal{L} ratio of the stellar disk does not change significantly with radius and that the dark halo can not be as flat as the stellar disk. Rupen (1991), using more sensitive and much higher resolution data, found that the width of the gaseous disks of NGC 891 and NGC 4565 increase exponentially, but for NGC 891 with large scatter. Our galaxy has been studied in much greater detail by Knapp (1987) and Merrifield (1992) in HI, and by Malhotra (1994) in CO. These authors find that the radial scale-length of the midplane mass density compares well with the radial scale-length of the stellar disk, implying a constancy of the mass-to-light ratio for the stellar disk.

Van der Kruit (1988) concludes that in the outer parts of stellar disks the local mass density is no longer dominated by the stellar disk so that the self-gravity of the gas will become important. Here I extend van der Kruit's pioneering work by incorporating the stellar and gaseous disks as well as the DM-halo in a self consistent way : rather than making a *local* approximation to the vertical force, K_z is calculated from the *global* mass distribution of the galaxy. In §3.2. I show that the self-gravity of the gas can play an important role and must be included in a self-consistent manner. Furthermore I will concentrate on the flaring behaviour in the region beyond the optical disk where the vertical force is dominated by the DM-halo, and is hence sensitive to its *shape*. In combination with the newly achievable large sensitivities and the high resolution of HI synthesis observations (Rupen, 1991), these improved modelling methods allow for the determination of the shape of dark halos of spiral galaxies.

In §2. I review some of the properties of dark halos and determine (in §2.1.) how, for a given rotation curve, the core radius and central density depend on the flattening of such an isothermal halo (see also Appendix A). The disk-halo conspiracy is investigated in section §2.2. (and Appendix B) where I

derive general formulas for the three unknowns (the disk’s \mathcal{M}/\mathcal{L} ratio and the halo’s core radius and central density) which determine the overall mass distribution of the galaxy. In §3. I list the assumptions made to determine the z -distribution of the gas from the galaxian potential. I compare the local and global approaches in §3.1., where I also present the vertical force arising from the total mass distribution of the galaxy, $K_{z,tot}$, for several radii (an analytic solution to the multi-component local approximation, as proposed by Bahcall (1984), is given in Appendix C). In §3.3. I calculate how the thickness of the gas layer depends on the two free parameters (\mathcal{M}/\mathcal{L} and q) and discuss how the thickness of the gas layer can be used to determine the flattening of the DM-halo. In the discussion, §4., I will indicate which systems might be suitable for an analysis as proposed in this paper.

2. Properties of dark halos

From the observational fact that rotation curves of spiral galaxies are “flat”, it has been concluded (e.g. Bosma 1978; Rubin *et al.* 1980; Bahcall & Casertano 1985; Begeman 1987) that there is an unseen mass component present in these galaxies. The standard assumption has been that this dark mass distribution is spherical and isothermal, characterized by the core radius, R_c , and central density, $\rho_{h,0}$ (equation [A1], with $q = c/a=1$). The luminous matter consists of a stellar disk, for some systems a bulge, and a gaseous disk. The \mathcal{M}/\mathcal{L} ratios of the bulge and the disk are free parameters but are normally taken to be constant with radius. An upper limit to the \mathcal{M}/\mathcal{L} ratio of the disk, and hence a lower limit to the dark halo mass, can be obtained by assuming that the observed peak rotation velocity is due to the stellar disk only. A more common approach is to scale the mass-to-light ratios down in such a way as to avoid halos with hollow cores. This is commonly known as the “maximum-disk” hypothesis (van Albada & Sancisi, 1986). Other means of constraining the \mathcal{M}/\mathcal{L} ratio exist : van der Kruit (1981) calculates \mathcal{M}/\mathcal{L} from the thickness of the gas layer, Efstathiou *et al.* (1982) invoke disk stability arguments, Athanassoula *et al.* (1987, ABP87) apply spiral instability criteria, and Bottema (1993) uses stellar velocity dispersion measurements. The mass-to-light ratios found by these authors range from 50 to 100 % of the maximum-disk value.

The values for the DM-halo core radius and the

\mathcal{M}/\mathcal{L} ratio of the stellar disk are highly correlated : low mass-to-light ratios require small core radii, and large \mathcal{M}/\mathcal{L} ratios correspond to large values for the DM-halo core radius. In fact, many different disk-halo decompositions produce acceptable fits to a given observed rotation curve (van Albada *et al.*, 1985 hereafter ABBS85 ; Persic & Salucci, 1988 ; Lake & Feinswog, 1989 hereafter LF89). The dark to luminous mass ratio may decrease with increasing mass (e.g. ABP87; Casertano & van Gorkom 1992; Broeils 1992, Chapter 10). This could be inferred from galactic rotation curves : dwarf galaxies have rising rotation curves (e.g. Carignan & Freeman 1988) while the rotation curves of massive galaxies fall in the outer parts (Casertano & van Gorkom 1991; Broeils 1992). For those galaxies where the rotation curves in the outer parts are flat, the luminous and dark matter “conspire” : the increase of V_{halo}^2 and the decline in V_{disk}^2 are such that their sum remains approximately constant with galactocentric radius.

In view of the uncertainties in the disk-halo decomposition, it is clear that more and a different kind of data are needed for a unique determination of the halo flattening. In section §3.3. I show that beyond the optical disk the thickness of the gas layer is rather sensitive to the flattening of the halo. In order to investigate this sensitivity quantitatively I construct a two parameter galaxy model, where these parameters are γ (= the fraction of the peak rotation curve due to the stellar disk, see §2.2. and Appendix B) and q , the flattening of the DM-halo (§2.1. and Appendix A). The explicit dependence of the thickness of the gas layer upon these two parameters is discussed in §3.3..

2.1. Flattened dark halos

As mentioned above, the equatorial rotation curve (i.e. the rotation curve in the plane of the stellar disk) does not constrain the actual shape of the halo. In Appendix A I determine a family of flattened DM-halo models which have the same (to within 1.4 %) equatorial but different polar rotation curves. Thus, for this family of halo models, the radial force does not depend significantly on the shape of the DM-halo, while the vertical force (and hence the thickness of the gas layer) does. In Figure 1, I present the rotation curves for this DM-halo family graphically. The lower panel shows the rotation curves for these DM-halo models, while in the top panel I present the ra-

tio of the flattened to the round DM-halo rotation curve. Although the residuals show systematic behavior, the amplitudes ($\leq 1.4\%$) are smaller than the routinely obtained observational errors (e.g. Bege-man 1989, BE89 hereafter; Broeils 1992). In conclusion : rotation curves of flattened DM-halos are indistinguishable from their round equivalents. This family of flattened DM-halo models is fully specified by the equations (A8) and (A9) which relate the core radius and the central density to the flattening of the DM-halo and is graphically presented in Figure 2. For a given rotation curve, flattened DM-halo models have larger core radii and central densities than their round equivalents. Notice that both the central density and the core radius have an almost linear dependence on the halo flattening for moderately flattened DM-halos.

Of course the DM-halo model I have chosen to work with might very well be different from the true DM halo mass distribution. However all mass distributions, with similar rotation curves, share the general feature that flatter distributions have larger vertical forces. Therefore, a DM halo flattening determined using the formalism outlined in this paper serves as an indicator of the true flattening of the (unknown) dark matter density distribution.

2.2. On the disk-halo conspiracy

As we can measure the light distribution of the stellar disk only, and have no a priori knowledge of the mass-to-light ratio of stellar disks, the relative contributions of luminous and dark matter are not known (ABBS85 and LF89). However, as I will show in Appendix B, the galaxy mass model described above is fully determined by *one* parameter regulating the relative importance of stars and dark matter. Following Bottema (1993) I choose this parameter, γ , to be the fraction of the peak observed rotation curve which is due to the stellar disk (defined by eqn. [B15]).

Different choices of γ result in quite different values for the stellar mass-to-light ratio, the halo's central density and core radius. As an example, I present the dependence of these three parameters on γ for the galaxy NGC 3198 (rotation curve and optical parameters were taken from BE89) in Figure 3, and algebraically by the equations (B16), (B18) and (B19). In Figure 3, I have also indicated how a 5% uncertainty in the slope of the rotation curve affects the results. To obtain the core radius and central density

of a flattened dark halo, one uses the equations (B18) and (B19) and multiplies these values by $\mathcal{C}(q)$ (equation [A8]) and $\mathcal{H}(q)$ (equation [A9]) respectively.

In agreement with LF89, I find that observed equatorial rotation curves do not constrain the core radius of the DM-halo (or γ in our terminology) very well. This is illustrated in Figure 4, where I present the rotation curve of a model galaxy which resembles the Sc galaxy, NGC 3198¹. Several acceptable fits, made with different γ 's, are shown.

In conclusion : the parameterization of the disk-halo conspiracy, as presented in Appendix B, provides a useful way to perform the disk-halo decomposition to acceptable accuracy, and allows for a straightforward way to investigate the dependence of the thickness of the gas layer on the γ value (mass-to-light ratio) of the stellar disk.

3. The method

In this section I derive the vertical distributions of the HI layer from the potential of the whole galaxy, $\Phi_{galaxy}(R, z)$, and the equation of hydrostatic equilibrium. This derivation is subject to several simplifying assumptions which are listed below :

- The system is in steady state,
- and is azimuthally symmetric.
- The velocity dispersion tensor of the gas is symmetric and round, so that
- The equation of hydrostatic equilibrium is a good approximation to the vertical Jeans equation.
- The vertical velocity dispersion of the HI gas is constant (isothermal) with z-height.
- Magnetic and cosmic ray pressures are neglected

Obviously this is just an approximate description of reality. Spiral density waves violate the first two

¹ The optical parameters ($L(0)=207.1 L_{\odot}/pc^2$, $h_R = 2.3$ kpc, $z_e = 0.23$ kpc), gaseous surface density distribution and rotation curve ($V_{obs}(2.3h_R) = 146.4$, $V_{obs}(10.0h_R) = 148.0$, $V_{gas}(2.3h_R) = 13.4$ and $V_{gas}(10.0h_R) = 38.0$ km/s) were taken from BE89 who used Kent's (1987) photometry to calculate the rotation curve due to the stellar disk. The stellar disk is truncated at $6h_R$ (van der Kruit, 1988).

assumptions, while non-thermal pressure terms (magnetic, cosmic ray heating, ...) are not included in the equation of hydrostatic equilibrium. Keeping these assumptions in mind, I take as the starting point the vertical Jeans equation in cylindrical coordinates (as usual, R , θ , and z denote the radial, the tangential and the vertical direction respectively) :

$$\frac{d(\rho(z)\sigma(R,z)_{zz}^2)}{dz} = \rho(z)K_z(z) - \frac{1}{R}\frac{\partial}{\partial R}(R\rho\sigma_{Rz}^2) - \frac{1}{R}\frac{\partial}{\partial\theta}(\rho\sigma_{\theta z}^2), \quad (1)$$

to determine the vertical distribution of the gas ($\rho(z)$). Here $K_z(z)$ is the gravitational force (per unit mass) in the $+z$ -direction and $\sigma(R,z)$ the gaseous velocity dispersion. Due to the assumption of azimuthal symmetry, the last term in equation (1) vanishes. The σ_{Rz} -term essentially measures the tilt of the velocity dispersion ellipsoid, for cylindrical rotation it is identically zero. In the most extreme case the velocity dispersion ellipsoid points towards the galactic center².

At small z/R , σ_{Rz} is approximately $(\sigma_{RR}^2 - \sigma_{zz}^2)z/R$ so that its contribution is expected to be small³. Thus, the non-diagonal terms of the velocity dispersion tensor (i.e. σ_{Rz}^2) will vanish. Then, the vertical Jeans equation reduces to the equation of hydrostatic equilibrium :

$$\frac{d(\rho_{gas}(z)\sigma(R,z)_{z,gas}^2)}{dz} = \rho_{gas}(z)K_z(z). \quad (2)$$

With the assumption that the gas is isothermal in the z -direction it follows that :

$$\sigma_{z,gas}^2 \frac{d \ln \rho_{gas}(z)}{dz} = -\frac{d\Phi_{galaxy}(R,z)}{dz}, \quad (3)$$

so that

$$\rho_{gas}(R,z) = \rho_{gas}(R,0)e^{-\Phi_{galaxy}(R,z)/\sigma(R)_{z,gas}^2} \quad (4)$$

$$\approx \rho_0 \exp(-z^2/2W_{gas}^2). \quad (5)$$

²I thank the referee, Phil Maloney, for pointing this out.

³In the Galaxy, σ_{RR} and σ_{zz} , as measured by Malhotra's (1994) and Blitz *et al.* (1984) are almost equal : 7.8 ± 3 versus 5.7 ± 1.2 km/s.

We see that the gaseous density distribution can be calculated once the gaseous velocity dispersion and the potential of the galaxy, $\Phi_{galaxy}(R,z)$, are known. Generally speaking, the vertical distribution of the gas will not be a "simple" function of z . Since the observational data does generally not allow for a more sophisticated analysis than the fitting of Gaussian functions to the measurements, I choose to fit Gaussians to the model density distributions (eqn. [4]) as well⁴. In the remainder of this paper I will use the dispersion (W_{gas}) of this Gaussian, as defined by eqn [5], as a measure of the width of the gas layer.

I incorporate three components in the present study : 1) a stellar disk with constant scale-height, 2) a flattened isothermal DM-halo, and 3) a gaseous disk. The stellar density distribution for the stars must be close to the one derived from surface brightness measurements by van der Kruit & Searle (vdKS81a&b and vdKS82a&b), namely :

$$\begin{aligned} \rho_s(R,z) &= \mathcal{M}/\mathcal{L} \rho_s(0,0) e^{-R/h_R} \operatorname{sech}^2(z/2z_e) \quad R \leq R_{max} \\ &= 0.0 \quad R > R_{max}, \end{aligned} \quad (6)$$

with $R_{max} = (4.7 \pm 0.7)h_R$, $2z_e \approx h_R/(4.7 \pm 1.8)$, and \mathcal{M}/\mathcal{L} the average mass per unit luminosity.

⁴ Since the *shape* of the potential changes with galactocentric radius, the gaseous density distribution will also change shape. Thus, the accuracy of the approximate density distribution (eqn. [5]) will also change with galactocentric radius. Other indicators for the width of the gas layer could be used as well. For example the normalized second moment of the density distribution, $W_{MOM2} = \sqrt{\int_{-\infty}^{+\infty} z^2 \rho(z) dz / \int_{-\infty}^{+\infty} \rho(z) dz}$, is more sensitive to the high- z parts of the density distribution, yielding *larger* values for the "width" of the gas layer. On the other hand, the width could be calculated from the Full Width at Half Maximum ($W_{FWHM} = FWHM/2.35$), a calculation which is more sensitive to the low- z part of the density distribution, so that *smaller* values for the "width" are found. Significant differences between these three width measures indicate that the true density distribution is not Gaussian. For the toy model discussed below the W_{FWHM} and W_{MOM2} width estimators can be as much as 20% larger and smaller than W_{gas} respectively (inside the optical disk). Beyond the optical disk, the gaseous distribution is close to Gaussian.

Note that Barteldrees & Dettmar 1993 (BD93) find that the optical disks are truncated at significantly smaller radii : $R_{max} = (3.0 \pm 0.2)h_R$, $2z_e \approx h_R/(4.0 \pm 0.3)$. In external galaxies it is very hard to observationally distinguish a sech-squared distribution from an exponential distribution (i.e. Wainscoat *et al.* 1989). For the Galaxy on the other hand, there is a large body of evidence suggesting that the vertical distribution can be better represented by an exponential distribution⁵ : $\rho_s(z) = \rho_s(0) e^{-z/z_e}$ (Gilmore & Reid 1983; Pritchett 1983; van der Kruit 1986; Yoshi *et al.* 1987). Therefore, I calculate model potentials for the exponential distribution. I chose the flattened isothermal distribution as proposed by SS90 (equation [A1]), discussed above, to represent the DM-halo mass distribution.

The vertical force of a truncated stellar disk as well as of a flaring disk is calculated from the potential :

$$\Psi(R, z) = -2G \int_0^\infty r dr \rho(r, 0) \int_{-\infty}^\infty dz' \rho(r, z') \int_0^\pi \frac{d\theta}{|\vec{r} - \vec{R}|} , \quad (7)$$

$$K_z(R, z) = -\frac{d}{dz} \Phi(R, z) \quad (8)$$

$$= -2G \int_0^\infty r dr \rho(r, 0) \int_{-\infty}^\infty dz' \frac{\rho(r, z')(z - z') f(R, z, r, z')}{\sqrt{(R+r)^2 + (z-z')^2} ([R-r]^2 + [z-z']^2)} , \quad (9)$$

where $\rho(r, z')$ is the density distribution for which to calculate the forces. At the center of the galaxy, $f(0, z, r, z')$ equals π , for all other galactocentric radii $f(R, z, r, z')$ is the complete elliptic integral of the second kind : $f = E(k) = \int_0^\pi d\phi \sqrt{1 - k^2 \sin^2 \phi}$, with $k^2 = 4r/[(1+r)^2 + (z-z')^2]$. With special care for the region around (R, z) this integral can be solved numerically and takes about 8 seconds per point on a SPARC 2 processor. I use an exponential for the vertical density distribution, $\rho(0, z')$, of the stars, while I approximate the gaseous distribution by a Gaussian. As neither the vertical scale-height nor the midplane density, $\rho(r, 0)$, are generally analytic functions, I store their values in tabular form and determine the interpolated value whenever the integrating routine (QROMB or QROMO, Press *et al.* 1990) requires so. I used the double exponential stellar disk (Kuijken & Gilmore, 1989, hereafter KG89, their eqn. [27]) as a test case and found that the two methods of calculation agree to within 1 part in 1,000⁶.

3.0.1. The global approach

As a first step I use the radial part of the potential to determine the structural parameters of the stellar disk and DM-halo by requiring that they reproduce the observed equatorial rotation curve. The radial force due to the gas is calculated (using the ROTMOD program in GIPSY, van der Hulst *et al.* 1992) assuming that it is infinitely thin. I use the observed photometry and a constant \mathcal{M}/\mathcal{L} ratio to calculate the rotation curve due to the stars (also by using ROTMOD). I then perform the disk-halo decomposition outlined in Appendix B.

I use the values for the mass-to-light ratio of the stellar disk and the core radius and central density of the DM-halo, as found in the disk-halo decomposition, to calculate the vertical force due to the stellar disk (equation [9]), and the DM-halo (SRJF94's equation [6]). These forces are integrated numerically to yield the potential, from which the gaseous volume density distribution, $\rho_{gas}(R, z)$, is calculated (using eqn. [4], an assumed gaseous velocity dispersion, and an observed surface density distributions).

I follow an iterative procedure, where the gaseous density distribution, calculated from an approximation to the true total potential, is used to estimate the gaseous contribution to the potential, which must then be added to the

⁵In this paper I do not include any thick disk component. Note that these isothermal and exponential vertical distributions have the same slope at large z-heights. Thus for a given surface density and high-z slope, the exponential distribution has a twice larger value of the midplane density than the isothermal distribution (see also van der Kruit, 1988).

⁶This accuracy equals ten times the accuracy obtained in the integrating routines.

contributions from the stellar disk and DM-halo to yield a better approximation to the true total potential, from which a better approximation to true gaseous density distribution can be calculated, ... etc.

Thus, the vertical distribution of the gas is not fully consistent with the Poisson equation

$$4\pi G \rho_{tot}(R, z) = -\frac{1}{R} \frac{\partial(R F_R)}{\partial R} + \frac{1}{R^2} \frac{\partial^2 \Phi}{\partial \phi^2} - \frac{\partial K_z}{\partial z}, \quad (10)$$

since I take the vertical distribution of the gas layer to be Gaussian, and because the radial force (F_R) due to a thick gas layer differs from the radial force arising from an infinitely thin disk. These inconsistency are expected to be small because of the small scale-height and low mass of the gaseous disk. This procedure to calculate the thickness of the gas layer is what I term the *global approach*.

In order for the global model to be self-consistent, the stellar velocity dispersion tensor ($\sigma(R, z)_{*,ij}^2$, with ij all the possible coordinate combinations) has to be such that for the assumed stellar density distribution and the calculated total potential, the vertical Jeans equation (1) will be satisfied. Thus, every mass model described above makes two predictions, firstly the radial variation of the width of the gaseous layer, and secondly the stellar velocity dispersion. In this paper I concentrate on the radial variation of the thickness of the gas layer.

3.1. The Local Approach

To date, most authors have determined the distribution of the gas above the plane from the *local* mass densities only. In this section I compare this local approach with the global approach described in the previous section. To separate variables I will postpone investigating the effects of the gaseous self-gravity till §3.2..

First I describe how in the local approach the vertical force is calculated from the local mass densities and gradients in the rotation curve. Assuming that, in the region where the gas is found, the rotation speed does not depend on z -height and that the vertical force does not depend on radius, the Poisson equation (10) reduces to the local Poisson equation:

$$4\pi G \rho(z) = -\frac{1}{R} \frac{d(R F_R)}{dR} - \frac{dK_z}{dz}. \quad (11)$$

Combining the appropriate equation of hydrostatic equilibrium (3) with the equation above (11) I find :

$$\sigma_{z,gas}^2 \frac{d \ln \rho_{gas}(z)}{dz} = -4\pi G \int_0^z dz' \left\{ \rho_{matter}(z') + \left(\frac{-2}{4\pi G} \right) \left(\frac{V_{rot}}{R} \frac{dV_{rot}}{dR} \right) \right\}.$$

Setting the rotation curve term to ρ_{rot} , it follows that :

$$\sigma_{z,gas}^2 \frac{d \ln \rho_{gas}(z)}{dz} = K_z(z) = -4\pi G \int_0^z dz' \{ \rho_{matter}(z') + \rho_{rot}(z') \}. \quad (12)$$

Negative and positive rotation densities (ρ_{rot}) correspond to rising and falling rotation curves respectively. The effect of a rising rotation curve is to increase the thickness of the gaseous and stellar disks, while in a falling rotation curve a disk will be thinner relative to the case where $\rho_{rot} = 0$. Bottema *et al.* (1987) find that the rotation term can contribute significantly in the rising parts of galactic rotation curves. For the case of a flat rotation curve, equation (9) leads to the plane-parallel-sheet case. Equation (12) can be solved either iteratively or analytically (if more simplifications are introduced) : the multi-component and Gaussian-equivalent methods described below.

3.1.1. The Gaussian equivalent method

In order to arrive at the (analytic) Gaussian-equivalent method, we simplify matters further by assuming that the self-gravity of the gas is negligible and that the total mass density does not vary significantly with height above the plane. I then arrive at :

$$\sigma_{z,gas}^2 \frac{d \ln \rho_{gas}(z)}{d z} = -4 \pi G \rho_{tot}(0) z,$$

so that the vertical distribution is Gaussian with dispersion $W_{gas,G}$:

$$\rho_{gas}(z) = \rho_{gas}(0) \exp(-z^2/2W_{gas,G}^2).$$

For which the following relation holds :

$$W_{gas,G} = \frac{\sigma_{z,gas}}{\sqrt{4 \pi G \rho_{tot}(0)}}. \quad (13)$$

In the Gaussian-equivalent method one then assumes that the Gaussian width ($W_{gas,G}$) can be equated with the observed width $W_{gas}(\approx FWHM/2.35$, as defined by eqn. [5]), so that the inferred midplane mass density (ρ_{inf}) is given by :

$$\rho_{inf} = \frac{1}{4\pi G} \left(\frac{\sigma_{z,gas}^2}{W_{gas}^2} \right). \quad (14)$$

Inside the stellar disk, the Gaussian width ($W_{gas,G}$) will always be smaller than the true width because, for any density distribution, the volume density decreases with z-height. The inferred midplane mass density, as calculated from the true width W_{gas} (which is larger than $W_{gas,G}$) and equation (14), will therefore underestimate the true midplane mass density. This effects is illustrated in Figure 5, where I plot the ratio of the inferred midplane mass density (ρ_{inf}) and the actual midplane density (ρ_{tot}). For several mass models resembling NGC 3198, this method recovers 50 to 110 % of the true midplane density. Especially for the round halo case ($q = 1.0$) we clearly see the effects of the truncation of the stellar disk at $R = 6h_R$. The truncation of the stellar disk of NGC 3198 occurs at a relatively large distance ($6h_R$ versus $4.7h_R$ on average, vdKS81a&b and vdKS82a&b, and BD93) so that it's effect may be relatively small for NGC 3198. On the other hand, the effects of the truncation of the stellar disk are smaller if the vertical distribution of the stars is sech^2 rather than exponential (i.e. less concentrated towards the midplane). It should be noted that these results depend somewhat on the

width estimator being used (see footnote 4), for example the radial variation of ρ_{inf}/ρ_{tot} arises partly because the vertical distribution of the gas gradually changes from a distribution which is strongly centrally peaked (in the inner two scale-lengths) to a Gaussian (beyond the optical disk).

Including the rotation density will improve the Gaussian-equivalent method beyond the truncation of the optical disk (right-hand side panel). The radial variation in the density ratio beyond the optical disk results from small scale structure in the model rotation curve. However, this is possible only if the sum of the rotation and DM densities is larger than zero (see eqn. [13] and Appendix C.). For example, this is *not* the case for a maximum-disk model of NGC 3198 in the inner two radial scale-lengths.

Although its accuracy varies systematically with radius, the Gaussian-equivalent method works reasonably well, especially beyond the stellar disk.

3.1.2. The plane parallel sheet case

The difference between the plane-parallel-sheet case and the global approach is most easily illustrated by plotting the vertical forces for the two cases. In Figure 6 I plot the $K_z(z)$ forces, as calculated for a NGC 3198-model, for a selection of radii. The dashed line is the vertical force due to a plane parallel sheet of stars with an exponential vertical distribution and a column density appropriate for the indicated radius. The open squares represent the force generated by a radially truncated exponential disk. The full line represents the $K_z(z)$ generated by the combined density distribution of the stellar disk and the DM-halo. For the combination of parameters, maximum-disk and round DM-halo (top-left panel), the plane-parallel-sheet case overestimates the vertical force in the inner two scale-lengths of the stellar disk, because the plane parallel sheet is a bad approximation to the fast radially declining surface density (there is very little surface area at the central surface density). Furthermore, the large negative ρ_{rot} associated with the steeply rising rotation curve (Figure 4) decreases the effective volume density. Beyond about $2 h_R$ the potential due to the interior stellar disk becomes more important and will eventually dominate the potential generated by the local column of stars. Additional model calculations (top-right panel : $\gamma = 0.9, q = 0.1$; bottom-left panel : $\gamma = 0.6, q = 1.0$; bottom-right panel : $\gamma = 0.6, q = 0.1$) show that the stellar disk has

a dominating contribution to the vertical force (over the extent of the stellar disk) if and only if the stellar disk is close to “maximum” and if the DM-halo is close to round (see also §B.4 and Figure 14).

3.1.3. Inferences

From the figures 5, 6 and 7 we learn the following :

—At large galactocentric radii ($R \geq 6h_R$), K_z is almost linear for the range of models considered here, resulting in an almost Gaussian vertical distribution for the gas. Notwithstanding the low stellar surface densities at these large distances, the contribution of the stellar disk to the total vertical force can be substantial : even at eleven radial scale-lengths the stellar disk contributes about 20 % of the total vertical force (for the round DM-halo cases). The self-gravity of the gas (see Figure 7), which is discussed in more detail in §3.2., can be important (up to 50% of the total force) in this region as well.

—In the transition region ($4h_R \leq R \leq 6h_R$) the contribution of the stellar disk, the gaseous disks, and the dark halo to the total vertical force can be of comparable magnitude (for the mass model with maximum disk, round halo, and typical gaseous surface densities. See Figure 7). Stellar disks are truncated (vdKS81a&b; vdKS82a&b; BD93) causing a sharp discontinuity in the stellar densities. However the potential as generated by the total stellar mass distribution will change much less abruptly. Thus the local approaches will strongly overpredict the thickness of the gas layer in this region (see Figure 5). Moving away from this corner ($\gamma = 0.9, q = 1.0$) in parameter space increases the halo’s contribution to the total potential significantly.

—Inside the optical disk, the potential is dominated by the stellar disk only in case the disk is close to “maximum” and the halo is almost round. For the other extreme case (minimum-disk+flat-halo), the potential is completely dominated by the DM-halo. In the two remaining corners of parameter space, stellar disk and DM-halo contribute about equally to K_z . In all of these cases, the density distribution of a tracer population will be almost Gaussian as long as the velocity dispersion of the tracer is so low that most of the tracer resides at z-heights below the “knee” in K_z (at two to three stellar scale-heights). For a tracer population like the atomic gas with a velocity dispersion of roughly 7 km/s, the entire extent of the optical disk falls in this regime (see Figure 10). Isothermal

tracers with a velocity dispersion larger than two or three times $\sigma_{z,gas}$ can move beyond the knee in the K_z curve so that their density distribution can no longer be adequately described by a single “simple” function (cf. the thick disk of the Milky Way [e.g. Gilmore & Reid 1983]).

—As expected, both the amplitude and the shape of the vertical force are almost independent of the γ value of the stellar disk if the DM-halo is highly flattened. In case of a round DM-halo, different γ values for the stellar disk do result in different shapes for the K_z curves.

As the amplitude of the knee in K_z depends linearly on central surface density (quadratically on $V_{rot,max}$, eqn. [B10]), the thickness of the gas layer will be smaller in high rotation curve galaxies and larger in dwarfs (see also Appendix D.).

Two radial regimes are poorly modeled by the Gaussian-equivalent as well as the plane-parallel-sheet local approaches : the region where the rotation curve rises so sharply that ($\rho_{rot} + \rho_{DM} < 0$), and the region where the stellar disk truncates. Special treatment of these regions can be avoided by using the global approach. For those regions where the rotation curve is almost flat, which are far away from the truncation of the stellar disk, the Gaussian-equivalent method works reasonably well.

3.2. The self-gravity of the gas

Rupen (1991) finds in NGC 891 as well as in NGC 4565, that the HI volume densities become comparable to the stellar volume densities beyond about 2 radial scale-lengths. For the Milky Way this is true at the solar circle. The self-consistent solution for the multi-component method as found in Appendix B.4. (eqn. [C28]) indicates that the importance of the self-gravity of the gas scales with the ratio of gaseous to stellar kinetic energy. At the solar circle this ratio is about 0.1-0.2, so that the self-gravity of the gas is expected to become increasingly important at larger radii.

The importance of the self-gravity of the gas is illustrated in Figure 7, where I plot the K_z due to the total (stars+DM+gas) potential (the full line), and the forces arising from the global DM, stellar and gaseous density distributions (dotted, short dashed, and long dashed lines respectively). The self-gravity of the gas has been calculated using the procedure outlined in §3.0.1..

3.2.1. The multi-component method

In case ρ_{rot} and the self-gravity of the gas are neglected it is rather straightforward to show (van der Kruit, 1988) that different isothermal components subject to the same cylindrically symmetric gravitational field have vertical distributions which are powers of each other. Including ρ_{rot} , the self-gravity of the gas, and the dark matter halo leads to the multi-component method, first used by Bahcall (1984) to determine the amount of disk-like dark matter in the solar neighborhood. In Appendix C., I present an analytic solution (eqn. [C28], which needs to be solved iteratively) to equation (12). In the same Appendix I also show that in the multi-component method the distribution of the gas is a power of the distribution of the stars as well. In Figure 9 I compare the model widths calculated in the multi-component method (where the vertical distribution of the stellar disk is fixed to a sech-squared, see Appendix C.) with those calculated using the global approach. The top plot shows the percentage difference between the global and local approaches. The structure in these difference curves mostly arises due to small scale structure in the observed rotation curve. Thus, application of the multi-component method could be misleading. For example, if the flaring measurements extend to a radius at which the local approach predicts a local maximum in the observable width, too round a DM-halo would be inferred.

I used the multi-component method to compare models of NGC 3918 with a varying amount of gaseous self-gravity. The results are presented in Figure 8. In the left-hand set of panels I show the width, $W_{gas}(\approx FWHM/2.35$, as defined by eqn. [5]), of the gas layer as a function of galactocentric radius for three different halo flattenings (bottom panel, $q = 1.0$; middle panel, $q = 0.5$; upper panel, $q = 0.1$). Four different curves are presented, the different lines corresponds to differently scaled gaseous surface densities : 1/100, 1, 5, and 10 times the measured surface density for the full line, the dotted line, the short dashed line and the long dashed line respectively. The models are calculated⁷ for a gaseous velocity dispersion of 7.5 km/s and a stellar disk with a γ value of 0.93 (i.e. about maximum-disk). For the scaled gaseous disks I plot (right-hand set of panels) the ratio of thickness of the

scaled disk and the thickness of the no-self-gravity-disk. From this plot we see that not including the gaseous self-gravity will result in an *overestimate* of the width of the gas layer (by approximately 10% to 20%). For the predicted gas-layer width to equal the observed widths a more massive DM-halo is required (eqn. [A9]), so that neglecting the self-gravity of the gas will result (using eqn. [14]) in a *smaller* value (by approximately 20% to 40%) for the halo flattening, q . Thus, in the local approach as well as in the global approach (see Figure 10), the self-gravity of the gas is found to have a comparable effect on the inferred DM-halo flattening.

From these plots I also conclude that for galaxies with relatively large gaseous surface densities the thickness of the gas-layer is not sensitive to the flattening of the dark matter at all. Thus, the self-gravity of the gas may be an unimportant or a significant contributor to the vertical force (for early and late type systems respectively).

3.3. Halo shape and gas layer thickness

In order to investigate the dependence of thickness of the gas layer upon the flattening of the DM-halo and the M/\mathcal{L} ratio of the stellar disk, I determined $\rho_{gas}(R, z)$ (and $W_{gas}(R)$ therefrom) for a range of galaxy models.

In Figure 10 I plot the width, $W_{gas}(\approx FWHM/2.35$, as defined by eqn. [5]), of the gas layer in a $\gamma = 0.9$ (i.e. \sim maximum-disk) disk-halo combination for several halo flattenings. The left-hand panel was calculated for a double exponential disk. In the middle panel I incorporated the truncation of the stellar disk (at $R/h_R = 6$), while the self-gravity of the gas is included in the right-hand panel. The effect of the self-gravity of the gas is different for the different disk-halo models, and is strongest between 4 and 8 radial scale-lengths : between 20% and 40% for the NGC 3198 models. Beyond several radial scale-lengths the width of the gas layer depends strongly (roughly proportional to \sqrt{q}) on the flattening of the DM-halo. Inside the stellar disk, the width of the gas layer is largely independent of the DM-halo flattening because the potential there is dominated by the stellar disk. However, for models with flatter halos and/or lower- γ stellar disks, the halo can be of importance inside the stellar disk (see §3.2.1., and Figure 6). It is important to keep in mind that the self-gravity of the gas is more important for

⁷The effect of the scaling of the gaseous surface density has been taken into account while performing the disk-halo decomposition.

the rounder DM-halo models (§3.2. and compare the Figures 7-a and 7-b). So the “signature” of the halo flattening is somewhat reduced if the self-gravity of the gas is important (see also Figure 8).

Is the thickness of the gaseous layer dependent on the mass-to-light ratio of the disk? In order to answer that question, I performed the calculations described above for several γ 's. The results (for $q = 1.0$) are presented in Figure 11. We see that, as expected, inside the stellar disk a gas-layer immersed in a more massive stellar disk will be comparatively thinner. At large galactocentric radii the thickness of the gas layer becomes virtually independent of the \mathcal{M}/\mathcal{L} ratio of the stellar disk. The same conclusion can be reached from Figure 5, where we see that, beyond the optical disk, the derived midplane mass densities for different \mathcal{M}/\mathcal{L} -disks are nearly equal.

3.4. Effects of incomplete modelling

It is instructive to see how uncertainties in gaseous velocity dispersion and uncertainties in the derivation of the vertical force affect our estimates of the DM-halo flattening. Another point of interest is to investigate what differences may arise when using the local instead of the global approach.

To summarize the following sections : the errors introduced by using the Gaussian-equivalent method (typically a 10-30% too round halo) tend to cancel out those introduced by neglecting the self-gravity of the gas (20-60% too flat a halo).

3.4.1. Uncertainties in the velocity dispersion

In many practical situations it may be that measurements of the gaseous velocity dispersion are not available. This severely limits our ability to determine the flattening of the DM-halo. In some face-on galaxies the azimuthally averaged gaseous velocity dispersion is observed to decline radially from around 12 km/s in the center to remain constant at 7 km/s beyond R_{25} (van der Kruit & Shostak 1982; Dickey *et al.* 1990). In other systems, the region beyond R_{25} , as well as the inter-arm regions appear to have a constant velocity dispersion of 7 km/s, while on the arms values around 13 km/s are reported, (Shostak & van der Kruit 1984; see Kamphuis 1993 for a review). In summary, the measurements to date indicate that the gaseous velocity dispersion beyond the optical disk has a value of around 7 km/s.

Overestimating the gaseous velocity dispersion by a factor of $(1+x)$ causes an overestimate of the midplane mass density by a factor of $(1+x)^2$. Beyond the optical disk, too flat a DM-halo distribution would be inferred (by the same factor $(1+x)^2$).

3.4.2. Uncertainties in the vertical force

Here I estimate the effects of neglecting certain components to the vertical force (e.g. the self-gravity of the atomic gas, magnetic forces, or the gravitational force due to some remote point source). A mass-model which uses an underestimate of the true vertical force requires a larger DM density and thus a smaller values of the halo flattening to reproduce the observed gas layer widths. Thus, underestimating the vertical force by a factor $(1+y)$ results in too small an estimate for the halo flattening (by a factor $[1+y]$). The inverse is true when working with an overestimate of the vertical force.

Neglecting the self-gravity of the neutral atomic gas, which can typically contribute 30 % to the vertical force (§3.2. and Figure 7), will result in a 30 % too small inferred halo flattening. Since the known molecular gas content of galaxies rarely exceeds 10% of the stellar mass (which contributes roughly 20% to K_z at large distances, see §3.1. and Figure 6), and is confined to the inner parts of the galaxy like the stars, I expect that neglecting the molecular gas will result in an underestimate of q by at most 2%.

3.4.3. Using the Gaussian-equivalent method

Application of the Gaussian-equivalent method to an observed set of gas layer widths underestimates the inferred midplane density by a radially varying amount (see §3.1., and Figure 5). As a result the inferred halos will be too round and have core radii that are too large.

4. Discussion and Conclusions

In the previous sections we have seen that a flattened dark halo imprints a very specific signature on the flaring of the gas-layer (Figure 10). Measurement of this flaring allows for the determination of the DM-halo flattening.

Although the global approach is limited by some of the same assumptions as the local approach (isothermality of the gas, zero non-thermal pressure terms,

constant \mathcal{M}/\mathcal{L} -ratio of the stellar disk, alignment between DM-halo and stellar disk, ...), it treats some other aspects much better (radial gradients in stellar surface density, the effects of the rising rotation curve, the non-cylindrical symmetry of the potential, ...). In particular the region where the rotation curve rises sharply and the region where the stellar disk truncates are better analyzed using the global approach. In those parts where the rotation curve is ‘flat’ and which are not too close to the truncation of the stellar disk the Gaussian-equivalent and multi-component methods can be used to reasonable accuracy. However, the global approach is less sensitive to small scale irregularities (Figure 9). To obtain reliable results, any applied method *must* include the self-gravity of the gas.

Therefore, I propose that the more robust global approach (§3.0.1.) should be used in programs aimed at determining the flattening of the dark matter halo. For a set of global mass distributions with varying halo flattening one can calculate the flaring behaviour of the gaseous disk. The DM-halo model exhibiting the best agreement between calculated and observed gas-layer widths then yields the halo flattening. The accuracy of the determined flattening can be gauged by varying the structural parameters of the individual mass components. Since the velocity dispersion of the gas is a crucial parameter in the analysis, care must be taken to determine its radial dependence. This will be done in a forthcoming paper where I will analyze the flaring gas layer of the almost edge-on galaxy NGC 4244.

4.1. Suitable systems

Nearby edge-on spiral galaxies with large (extending beyond the optical disk) neutral hydrogen envelopes are possible targets for studies of this kind. Symmetric systems are preferred since it is more likely that such systems are in equilibrium. Furthermore suitable systems should not exhibit strong warping. For systems with moderate warps, the kinematical information can be used to disentangle flaring from warping. Unfortunately these kind of systems might be rare.

In order to investigate the possibility of determining the thickness of the gas-layer in less inclined systems, I simulated HI observations of two models similar to NGC 3198 (inclined by 72° w.r.t. the line of sight). In the thin disk model, I constrained the gas-

layer to have a FWHM of 100 pc everywhere, while in the flaring disk model the gas-layer has a vertical distribution calculated using the multi-component method (including the self-gravity of the gas, eqn. [C28]). Both models were calculated with a gaseous velocity dispersion of 7.5 km/s. For a given set of observational parameters (15'' beam [\rightarrow 700 pc] and 2.56 km/s velocity resolution) I calculate the intensities originating from all points in the model galaxy for all velocities. Taking the normalized second moment with respect to radial velocity yields the apparent velocity dispersion for all points in the model galaxy. In Figure 12 I present the two model velocity dispersion maps. The systematic differences, of the order of 5 km/s, arise due to the fact that a line of sight through a flaring disk samples a wider range in position angle and galactocentric radius than the line of sight through a thin disk. In principle, the gaseous velocity dispersion can be determined after the layer-thickness-effects are corrected for. The thickness of the gas layer can be derived by comparing individual channel maps⁸. Contour maps of a particular channel are presented in Figure 13 : in the top panel the thin disk map is shown, the middle panel shows the thick disk equivalent while the difference between the two is contoured in the lower panel. Due to its larger vertical scale-height, the projected width of the thick-disk channel map should be larger than that of the thin-disk, while the average surface brightness will be reduced. This signature of the thick disk is easily recognized in the displayed contour maps. Furthermore, contrary to edge-on galaxies, the flaring can be measured in many different channel maps so that local irregularities (e.g. spiral streaming motions, bubbles, ...) are less likely to hamper the determination of the radial behaviour of the flaring (cf. Olling & van Gorkom, 1995).

Therefore I expect that it must be possible to experimentally determine both the gaseous velocity dispersion and the thickness of the gas-layer for moderately inclined systems as well.

4.2. A control sample

It might be possible to test the importance of neglected physics in galaxies where the rotation curve falls in Keplerian manner. In such systems the con-

⁸A channel map is an image (of a galaxy) taken in a “narrow band filter” : 2.56 km/s wide in this case.

tribution of the dark matter to the global potential is presumably small, thereby eliminating the gas layer thickness dependence on the shape of the DM-halo. As a result the thickness of the gas layer should depend on the total visible mass of the galaxy and the gaseous velocity dispersion only. Some galaxies exhibit falling rotation curves, albeit not in Keplerian manner (Casertano & van Gorkom 1991; Broeils 1992).

The measured width of the gas layer can then be compared with model predictions. If the gas layer is observed to be thicker than predicted, one might conclude that magnetic and cosmic ray pressures are important. On the other hand, a gas layer thinner than predicted indicates that either the ionizing extra-galactic radiation field is important (e.g. Maloney 1993), or that an unseen disk-like DM component is present (i.e. the “clumpuscles” proposed by Pfenniger *et al.* 1994a, and Pfenniger & Combes 1994b).

4.3. Summary

I have investigated the use of accurate determination of the thickness of the HI-layer in external galaxies. In combination with constraints set by the gaseous velocity dispersion and the rotation curve, I find that in principle it is possible to determine the shape of DM-halos. The gaseous self-gravity contributes significantly to the vertical force field (up to 40%) but can be modeled accurately using the global approach (§3.0.1.) outlined in this paper. The thus determined halo flattening is independent of the particular choice of disk-halo decomposition.

In practice (not necessarily edge-on) systems with extended HI-disks and regular velocity fields should be used, provided that they are observed with high angular and velocity resolution.

I would like to thank Jacqueline van Gorkom for the support, encouragement and stimulating discussions during my years in graduate school. Michael Rupen’s work initiated this line of research : the many discussions we had over the years and his comments on an earlier version of this paper were of great help to me. Furthermore I would like to thank HongSheng Zao who reminded me of quite a few analytic tricks applied in Appendix C. Penny Sackett helped me a lot by providing me with the relations for K_z and F_R of flattened DM-halos. I want to thank Kevin Pren-

dergast for his suggestion to investigate the global approach and his careful reading of an earlier version of the manuscript. David Schiminowich, as an unprejudiced reader, provided useful tips for improvement. I also thank Phil Maloney, the referee, for some useful suggestions to improve this paper. And finally I would like to thank NRAO and the Kapteyn Astronomical Institute for developing and maintaining the AIPS and GIPSY software packages respectively.

This work was supported in part through an NFS grant (AST-90-23254 to J. van Gorkom) to Columbia University.

Appendices

A. Rotation curves of flattened DM-halos

As mentioned before, it is not possible to constrain the DM-halo flattening by measurements of the equatorial rotation curve since both round and flattened mass distributions can generate the same rotation curve. In this Appendix I show that the DM-halo model used by Sackett & Sparke (1990) :

$$\rho_h(R, z; q) = \rho_{h,0}(q) \left(\frac{R_c(q)^2}{R_c(q)^2 + R^2 + (z/q)^2} \right), \quad (\text{A1})$$

(where R_c , $\rho_{h,0}$ and $q (= c/a)$ are the DM-halo core radius, central density and flattening respectively) defines a one-parameter family of halo models with essentially the same equatorial rotation curve if core radius and central density depend in a specific way on this one parameter, q (equations [A8] and [A9] respectively).

SRJF94 give a general relation for both the vertical and the radial force due to such a dark halo (their equation [6]). Evaluating this relation in the midplane, I find that the equatorial rotation curve arising from a flattened DM-halo is given by :

$$V_{halo}^2(R; \rho_{h,0}, R_c, q) = V_{halo}^2(\infty; \rho_{h,0}, R_c, q) \times Q(R; R_c, q), \quad (\text{A2})$$

with

$$Q(R; R_c, q) = \left\{ 1 - \left(\frac{g(q)}{\arctan g(q)} \right) \left(\frac{q^2 R_c^2(q)}{R^2 + (1 - q^2) R_c^2(q)} \right) \arctan \left(\frac{R^2 + (1 - q^2) R_c^2(q)}{q^2 R_c^2(q)} \right) \right\}, \quad (\text{A3})$$

and

$$V_{halo}^2(\infty; \rho_{h,0}, R_c, q) = 4\pi G \rho_{h,0}(q) R_c^2(q) f(q), \quad (\text{A4})$$

while $f(q)$ and $g(q)$ are given by :

$$f(q) = \left(\frac{q \arccos q}{\sqrt{1 - q^2}} \right) \quad g(q) = \left(\frac{\sqrt{1 - q^2}}{q} \right). \quad (\text{A5})$$

It is easily verified that equation (A2) indeed yields the familiar $V_h^2(R) = V_h^2(\infty) \{1 - (R_c/R) \arctan(R/R_c)\}$, the rotation curve due to a round halo.

Changing the flattening of the halo should not change the halo rotation curve significantly, that is to say : $V_{halo}^2(R; q) \approx V_{halo}^2(R; 1)$ for all radii. Noting that $f(1) = 1.0$, I find that at infinity the following relation holds :

$$\rho_{h,0}(1) R_c^2(1) = \rho_{h,0}(q) R_c^2(q) \times f(q). \quad (\text{A6})$$

Requiring that the round-halo rotation curve equals the flattened-halo rotation curve at $R = R_c(q)$ leads to the following relation :

$$\left(1 - \frac{R_c(1)}{R_c(q)} \arctan \frac{R_c(q)}{R_c(1)}\right) = \left\{1 - \left(\frac{g(q)}{\arctan g(q)}\right) \left(\frac{q^2}{2 - q^2}\right) \arctan \left(\frac{2 - q^2}{q^2}\right)\right\}. \quad (\text{A7})$$

Noting that the RHS of this equation varies between 1.28 and 1.00 for $q \in [0.1, 1.0]$, so that $R_c(q)/R_c(1)$ is constrained to the interval $[1.00, 1.242]$, I expand (to second order) the left-hand and right-hand sides of this equation with respect to $R_c(q)/R_c(1)$ and q respectively. The resulting quadratic equation is solved to obtain the core radius of the DM-halo as a function of flattening. The central density is then found from equation (A6). After substituting the solutions for $R_c(q)$ and $\rho_{h,0}(q)$ in the equation for the rotation curve (equation [A2]) it is found that the rotation curves of flattened DM-halos reproduce the rotation curve of a round halo to within 7 % (for $q = 0.2$). This error is maximal for $R = 0$, changes sign at $R = R_c(q)$ and slowly drops from -2% at two core radii to 0% at infinity. Since these deviations are large in the region where rotation curves are determined, such accuracy is not acceptable for our purpose. A little experimentation leads to a solution which is more acceptable : our best approximation (errors $\leq 1.4\%$) to the dependence of halo core radius and central density on its flattening q is graphically presented in Figure 2 and algebraically below :

$$\begin{aligned} R_c(q) &= R_c(1) \times (1.209 - 0.332q + 0.123q^2) \\ &= R_c(1) \times \mathcal{C}(q), \end{aligned} \quad (\text{A8})$$

and

$$\begin{aligned} \rho_{h,0}(q) &= \rho_{h,0}(1) \times \left(\frac{1}{f(q)\mathcal{C}(q)^2}\right) (0.954 + 0.0533q - 0.0073q^2) \\ &= \rho_{h,0}(1) \times \mathcal{H}(q) \quad \approx \quad \left(\frac{\rho_{h,0}(1)}{q}\right), \end{aligned} \quad (\text{A9})$$

where $\lim_{q \rightarrow 1} R_c(q) = R_c(1)$ and $\lim_{q \rightarrow 1} \rho_{h,0}(q) = \rho_{h,0}(1)$. Substituting (A9), (A8) and (A5) into equation (A1), I find that at large distances the local DM-halo densities are roughly proportional to $1/f(q) \approx 1/q$.

B. On the Disk-Halo conspiracy

In order to calculate the potential of the galaxy, the mass distributions of both the stellar disk and the DM-halo need to be parameterized in a convenient way. In this section I describe how the DM-halo structural parameters are related to those of the stellar disk. Given the photometry of the stellar disk and the observed rotation curve, a disk-halo mass model is fully determined by *one* parameter which regulates the relative importance of stars and dark matter. Following Bottema (1993) I choose the parameter, γ , to be the fraction of the peak observed rotation curve which is due to the stellar disk (defined by eqn. [B15]). With such a parameterization of the disk-halo decomposition available, it is

possible to investigate the effects of the stellar mass-to-light ratio upon the flaring of the gas layer. In accordance with van ABBS85 and LF89, I find that a wide range of stellar mass-to-light ratios (γ 's) produce acceptable “fits” to observed rotation curves.

Since the light distribution of the stellar disk is relatively well known, the first step in tackling the disk-halo conspiracy is the description of the rotation curve due to the stellar disk. When assuming a constant mass-to-light ratio, the stellar density distribution can be described, to first order, as radially exponential and vertically thin. The amplitude of the rotation curve due to such a thin exponential stellar disk depends only on its central surface density and radial scale length. The *shape* is fully determined by the radial density distribution. Casertano (1983) has shown that both the amplitude and shape of stellar rotation curves are sensitive to the thickness of the stellar disk as well as to the truncation radius, R_{max} (vdKS81a&b; vdKS82a&b; BD93). Therefore, the disk-halo conspiracy too will vary with the details of the stellar mass distribution. While the amplitude of the inner stellar rotation curve depends rather strongly on the thickness of the stellar disk, the outer rotation curve is virtually independent thereof. I will now investigate the dependence of the stellar rotation curve on the structural parameters of the stellar disk (h_R , R_{max} , and z_e).

I calculated stellar rotation curves, using the program ROTMOD in GIPSY (van der Hulst *et al.* 1992), for several truncation radii and disk thicknesses, and vertical distributions. As it turned out, the rotation curves of such stellar disks can be parameterized by a rotation speed at an inner (R_{inn}) and an outer ($R_{out} = x R_{inn}$) radius :

$$V_{rot,stars}^2(R_{inn}) = f_m \pi G h_R L(0) \mathcal{M}/\mathcal{L} \quad (\text{B10})$$

$$V_{rot,stars}(R_{out}) = f_x V_{rot,stars}(R_{inn}), \quad (\text{B11})$$

where $L(0)$ is the central surface brightness, \mathcal{M}/\mathcal{L} the mass-to-light ratio, and h_R the radial scale length of the stellar disk. I take $R_{inn} = 2.3h_R$, because a typical stellar disk (truncated at $4.5h_R$ and $h_R/z_e = 0.1$) has its maximum rotation speed at this distance. The constants f_m and f_x depend upon the the vertical distribution and the radial truncation of the stellar disk. For the outer radius I used three different values, $6.0h_R$, $8.0h_R$ and $10.0h_R$. The results are presented in Table 1 below for a range in parameters covering the observed range in thickness and truncation radius (vdKS81a&b; vdKS82a&b; Bottema *et al.* 1987; BD93).

The listed values are the average of the rotation curves for a vertically exponential and a vertically sech² stellar disk. With this choice for the two vertical distributions, sech-squared and exponential, I bracket the suggested range of suggested distributions (van der Kruit, 1988). The uncertainty concerning the true vertical distribution translates directly into uncertainties, Δf , in f_m and f_x . Experimentally I find, $\Delta f_m \approx (2\Delta f_6) \approx (2\Delta f_8) \approx (2\Delta f_{10}) = 0.6\%$, 1.2% , 1.7% and 2.3% for $z_e/h_R = 0.05$, 0.10 , 0.15 and 0.20 respectively), so that $f^{exp} = f + \Delta f$ and $f^{sech2} = f - \Delta f$. Thus, if the structural parameters of the stellar disk are well known the errors on the f -values are small. In situations where the thickness of the stellar disk are not known (as for all non edge-on systems) one must use the average values, $\overline{f_m}$ and $\overline{f_x}$, which are listed in the columns labeled “ $z_e/h_R = averaged$ ”. The uncertainties on these averages are typically 4.5, 2.0, 2.0 and 2.0 %. If also no information is available on the location of the truncation radius, then f_m , f_6 , f_8 , and f_{10} should be representative of the range in allowed values : I suggest $f_m = 0.73 \pm 6\%$, $f_6 = 0.68 \pm 10\%$, $f_8 = 0.57 \pm 10\%$ and $f_{10} = 0.50 \pm 10\%$.

B.1. The mass-to-light ratio of the stellar disk

Now I turn to the dark halo contribution to the observed rotation curve. As usual, the (square of the) observed rotation curve is generated by the quadratic sum of the constituting mass components :

$$V_{rot,obs}^2(R) = V_{rot,stars}^2(R) + V_{rot,bulge}^2(R) + V_{rot,gas}^2(R) + V_{rot,halo}^2(R). \quad (\text{B12})$$

Now I define the gas-bulge-corrected observed rotation speed as the square root of (B13).

$$\mathcal{V}_{rot,obs}^2(R) = V_{rot,obs}^2(R) - V_{rot,bulge}^2(R) - V_{rot,gas}^2(R), \quad (\text{B13})$$

so that :

$$\mathcal{V}_{rot,obs}^2(R) = V_{rot,stars}^2(R) + V_{rot,halo}^2(R). \quad (\text{B14})$$

Furthermore I define γ and β_x (= the slope of the rotation curve) :

$$\gamma = \frac{V_{rot,stars}(2.3h_R)}{\mathcal{V}_{rot,obs}(2.3h_R)} \quad \beta_x = \frac{\mathcal{V}_{obs}(x h_R)}{\mathcal{V}_{obs}(2.3h_R)}. \quad (\text{B15})$$

Given the observed radial scale length and central surface brightness of the stellar disk, the mass-to-light-ratio is a function of the stellar contribution to the peak rotation curve (γ) only and is given by (from the equations [B10] and [B15]) :

$$\mathcal{M}/\mathcal{L}(\gamma) = \left(\frac{\mathcal{V}_{obs}^2(2.3h_R)}{f_m \pi G h_R L(0)} \right) \times \gamma^2 = 10.25 \left(\frac{\mathcal{V}_{obs,100}^2(2.3h_R)}{f_{m,0.722} h_{R,1} L_{100}(0)} \right) \times \gamma^2, \quad (\text{B16})$$

where $\mathcal{V}_{obs,100}(2.3h_R)$ is the gas-bulge-corrected observed rotation speed at 2.3 radial scale-lengths in units of 100 km/s, $L_{100}(0)$ is the central surface brightness of the stellar disk in units of $100 L_\odot/\text{pc}^2$, $h_{R,1}$ is the radial scale-length in units of 1 kpc and $f_{m,0.722}$ in units of 0.722 (the f_m -value appropriate for a typical stellar disk with $h_R/z_e = 10.0$ and $R_{max}/h_R = 4.5$).

B.2. The core radius of the DM-halo

For a given observed rotation curve and a calculated stellar rotation curve *shape*, the core radius is determined uniquely by γ . Applying equation (B14) at 2.3 and $x h_R$, eliminating the terms depending on the stellar rotation curve, and using equation (A2) with $q = 1$, I find that the following relations hold :

$$\begin{aligned} \left(\frac{(\beta_x^2 - (f_x \gamma)^2)}{1 - \gamma^2} \right) &= \left(\frac{V_{rot,halo}^2(x h_R)}{V_{rot,halo}^2(2.3h_R)} \right) \\ &\approx a_{x,0} + a_{x,1} \left(\frac{R_c}{h_R} \right) + a_{x,2} \left(\frac{R_c}{h_R} \right)^2. \end{aligned} \quad (\text{B17})$$

The approximation (B17) is valid for small ranges in R_c/h_R only. I list these ranges, together with the ranges for the left-hand side of (B17) and the appropriate a_x -values in Table 2. These piecewise approximations recover the right-hand side of equation (B17) to within 0.2 %. No effort has been made to match the pieces smoothly.

For any assumed γ and measured β_x and f_x one can calculate the left-hand side of equation (B17) and find the appropriate a_x -values in Table 2 from which $\mathcal{R}_c = R_c/h_R$ follows :

$$\begin{aligned} \left(\frac{R_c}{h_R}\right) (\gamma; \beta_x, f_x) &\approx \frac{(-a_{x,1} + \sqrt{(a_{x,2})^2 - 4a_{x,2}}(a_{x,0} - l h s_x))}{2a_{x,2}} \\ &= \mathcal{R}_c(\gamma). \end{aligned} \tag{B18}$$

B.3. The central density of the DM-halo

The DM-halo central density is calculated from (B14), (B15) and (B18). With

$$\mathcal{V}_{obs}^2(2.3h_R) = \gamma^2 \mathcal{V}_{obs}^2(2.3h_R) + V_{halo}^2(2.3h_R) = \left(\frac{1}{1-\gamma^2}\right) V_{halo}^2(2.3h_R),$$

it follows that

$$\begin{aligned} \rho_{h,0}(\gamma; \beta_x, f_x) &= (0.185 M_\odot/\text{pc}^3) \left(\frac{\mathcal{V}_{obs,100}(2.3h_R)}{h_{R,1}}\right)^2 \times \\ &\quad \left\{\frac{(1-\gamma^2)}{\mathcal{R}_c(\gamma)^2}\right\} \left\{1 - \left(\frac{\mathcal{R}_c(\gamma)}{2.3}\right) \arctan\left(\frac{2.3}{\mathcal{R}_c(\gamma)}\right)\right\}^{-1}, \end{aligned} \tag{B19}$$

where \mathcal{R}_c , the normalized core radius of the DM-halo, depends strongly upon the choice for γ , and only weakly upon the shape of the rotation curve (via β_x) and the shape of the stellar mass distribution (via f_x).

As an example I present the dependence of the mass-to-light ratio of the stellar disk (lower right panel of Figure 3), the central density (upper left panel) and core radius (lower right panel) of the DM-halo on γ for NGC 3198 (photometry and rotation curve taken from BE89). The error-bars were calculated assuming the most common observational status : the truncation radius of the stellar disk is known but the thickness of the stellar disk is not. In this case, the accuracy with which one can determine the mass-to-light ratio of the stellar disk and the central density and core radius of the DM-halo are typically 3, 0.5 and 4 % respectively. If the thickness of the stellar disk is also known (as would be the case for edge-on galaxies), the errors decrease substantially, while they blow up if neither the truncation radius nor thickness of the stellar disk are known. For galaxies which are about “maximum-disk”, and have more or less flat rotation curves, Figure 3 shows that the core radius of the DM-halo will be $7 \pm$ (a factor of two) times the radial scale-length of the stellar disk, not too different from the maximum-disk-fits performed on real galaxies (Broeils 1992). Note that while the core radius of the dark halo approaches infinity as γ nears unity, the dark to luminous mass (upper right panel) is not singular.

I tested the procedure outlined above on simulated data, where I added (in quadrature) a stellar and a DM-halo rotation curve to represent a simulated total rotation curve. For falling, flat, as well as for rising simulated total rotation curves I was able to accurately recover the input parameters, provided that the slope of the total rotation curve is determined over as large a range in radius as possible.

As already pointed out by ABBS85 and LF89, mass models with a range (a factor of ten in some cases) in stellar mass-to-light ratios are consistent with observed rotation curves. I find, attempting to fit model rotation curves with “faulty” γ values (or \mathcal{M}/\mathcal{L} -ratios) that a wide range of stellar mass-to-light ratios is possible if small ($\approx 2\%$) differences between input and recovered rotation curves are allowed to occur. The differences between input and recovered rotation curves increase significantly inside the inner point and beyond the outer point which were used for to determine the slope of the rotation curve. This is illustrated in Figure 4 where I show the resultant fits to the observed rotation curve of NGC3198 (BE89) for several γ 's. I took the outer radius at 10 radial scale lengths. Although all γ values between 0.93 and 0.53 produce similarly acceptable fits, the low- γ -disks proposed by Bottema (1993) “fit” somewhat better. Since the velocity field of the inner parts of NGC 3198 deviates from circular rotation (Corradi *et al.*, 1991), the discrepancies between observed and model curves (in the inner parts) can not be used as an indication of goodness of fit.

Thus the method presented above presents us with an easy way to analyse many possible disk-halo decompositions. To obtain the core radius and central density of a flattened dark halo, one uses the equations (B18) and (B19) and multiplies these values by $\mathcal{C}(q)$ (equation [A8]) and $\mathcal{H}(q)$ (equation [A9]) respectively.

B.4. The Edge of the Optical Disk

Combining the relations for the \mathcal{M}/\mathcal{L} -ratio, the DM-halo core radius and central density it follows that :

$$\frac{\rho_{stars}(r)}{\rho_h(r)} = 27.7 \left(\frac{h_R/z_e}{10} \right) \left(\frac{0.722}{f_m} \right) \left(\frac{\gamma^2}{1-\gamma^2} \right) \times e^{-r} \times \left\{ \left(\mathcal{R}_c(\gamma)^2 + r^2 \right) \left[1 - \left(\frac{\mathcal{R}_c(\gamma)}{2.3} \right) \arctan \left(\frac{2.3}{\mathcal{R}_c(\gamma)} \right) \right] \right\}, \quad (\text{B20})$$

where $r = R/h_R$. Thus the ratio of stellar to DM midplane densities is independent of the *amplitude* of the observed rotation curve and depends only weakly on the *shape* of the rotation curve (via β_x), the truncation radius and thickness of the stellar disk (via f_m and f_x and h_R/z_e). The dependence of $\rho_{stars}(r)/\rho_h(r)$ upon galactocentric radius is graphically presented in Figure 14 for several γ values (full line $\gamma=0.9$, dotted line $\gamma = 0.8$, short dashed line $\gamma = 0.7$, long dashed line $\gamma = 0.6$, dash-dotted line $\gamma = 0.5$). I term the distance at which the disk densities no longer dominates⁹ the total midplane densities, R_{dde} . The maximum-disk like models have R_{dde} values ranging from four to seven, corresponding to the range where some stellar disks are observed to be truncated (vdKS81a&b; vdKS82a&b). Furthermore we notice that the luminous-to-dark matter ratio decreases rapidly with decreasing γ and q values.

⁹i.e. become smaller than a few times the DM density.

Recently Barteldrees & Dettmar (1993) have found that some spirals have edges in their light distribution as close in as two radial scale-lengths. Only for substantially rising rotation curves (say $\beta \geq 1.3$) and/or small γ values does R_{dde} become as small as two, suggesting that these systems have rising rotation curves and/or are DM dominated.

C. A self-consistent solution for the multi-component method

In this Appendix, from the equation of hydrostatic equilibrium (12), I derive a self-consistent analytical solution for the vertical distribution of the gas for the multi-component method proposed by Bahcall (1984). The solution (equation [C28]) is in the form of an integral equation for $z(\rho_{gas})$, which may be inverted numerically to yield $\rho_{gas}(z)$. This equation can be used, in an iterative manner, to determine the local dark matter density. The model galaxies presented in the Figures 8, 12 and 13 were calculated using this analytic method. As it turns out, an analytic solution can be found if one makes the approximation that the DM-halo density is constant with height above the plane in the region where the gas is co-spatial with the DM-halo. For DM-halos which are not too flattened this is not a bad approximation for most galactocentric radii. For the gas as well as for the stars the following equation holds :

$$\sigma_{z,i}^2 \frac{d \ln \rho_i(z)}{d z} = -4\pi G \int_0^z \{ \rho_{gas}(z') + \rho_{stars}(z') + (\rho_{halo} + \rho_{rot}) \} dz' . \quad (C21)$$

The density and dispersion (ρ_i and $\sigma_{z,i}^2$) can represent any isothermal component i , stars or gas. Since the right hand side of (C21) is the same for stars and gas, it follows that the vertical distributions are powers of each other. The density distribution has to be normalized such that the integral equals the surface density. So I write :

$$\rho_{gas}(z) = C_g (\rho_{stars})^{p_{sg}} = \rho_{gas}(0) \left(\frac{\rho_{stars}(z)}{\rho_{stars}(0)} \right)^{p_{sg}} , \quad (C22)$$

with

$$p_{sg} = \frac{\sigma_{stars}^2}{\sigma_{gas}^2} \quad \text{and } C_g \text{ such that} \quad \Sigma_{gas} = \int_{-\infty}^{+\infty} \rho_{gas}(z') dz' .$$

Similar relations can be defined for ρ_{stars} . Differentiating (C21) with respect to z yields :

$$A_{gas} \frac{d^2 \ln \rho_{gas}(z)}{d z^2} = \rho_{gas}(z) + \rho_{stars}(z) + (\rho_{halo} + \rho_{rot}) , \quad (C23)$$

with

$$A_{gas} = -\frac{\sigma_{z,gas}^2}{4\pi G} . \quad (C24)$$

Solving for the gaseous component after defining $\alpha(z) = \ln \rho_{gas}(z)$ I rewrite (C23) :

$$A_{gas} \frac{d^2 \alpha(z)}{dz^2} = e^\alpha + C_s (e^\alpha)^{p_{gs}} + (\rho_{halo} + \rho_{rot}) . \quad (C25)$$

Multiplying (C25) by $2 \frac{d\alpha}{dz}$ and using the equality : $\frac{d}{dz} \left(\frac{d\alpha}{dz} \right)^2 = 2 \frac{d\alpha}{dz} \frac{d^2\alpha}{dz^2}$, this equation reduces to :

$$A_{gas} \frac{d}{dz} \left(\frac{d\alpha}{dz} \right)^2 = 2 \frac{d\alpha}{dz} \{ e^\alpha + C_s (e^\alpha)^{p_{gs}} + (\rho_{halo} + \rho_{rot}) \} .$$

Integrating the RHS with respect to α yields :

$$A_{gas} \frac{d}{dz} \left(\frac{d\alpha}{dz} \right)^2 = 2 \frac{d}{dz} \left\{ e^\alpha + \frac{C_s}{p_{gs}} (e^\alpha)^{p_{gs}} + (\rho_{halo} + \rho_{rot}) \alpha + C \right\} .$$

For any physical system, the restoring force vanishes at the midplane (i.e. the RHS of [C21] equals zero), so that $\left. \frac{d\alpha}{dz} \right|_{z=0} = 0$. Thus the integration constant C is given by :

$$C = -\rho_{gas}(0) \left\{ \left(1 + \rho'_{s,g} p_{sg} \right) + (\rho'_{h,g} + \rho'_{r,g}) \ln \rho_{gas}(0) \right\} , \quad (C26)$$

where the primed variables are defined as follows :

$$\rho'_{s,g} = \frac{\rho_{stars}(0)}{\rho_{gas}(0)} ; \quad \rho'_{h,g} = \frac{\rho_{halo}(0)}{\rho_{gas}(0)} ; \quad \rho'_{r,g} = \frac{\rho_{rot}(0)}{\rho_{gas}(0)} . \quad (C27)$$

Thus :

$$\begin{aligned} \sqrt{\frac{-2}{A_{gas}}} \left\{ - \left(\rho_{gas} + \frac{C_s}{p_{gs}} (\rho_{gas})^{p_{gs}} + (\rho_{halo} + \rho_{rot}) \ln \rho_{gas} + C \right) \right\}^{+0.5} \\ = \frac{d\alpha}{dz} . \end{aligned}$$

Rearranging terms and integrating yields :

$$\sqrt{\frac{A_{gas}}{-2}} \int_{\rho_{gas}(0)}^{\rho_{gas}(z)} \frac{d\rho_{gas}}{\rho_{gas}} \left\{ - \left(\rho_{gas} + \frac{C_s}{p_{gs}} (\rho_{gas})^{p_{gs}} + (\rho_{halo} + \rho_{rot}) \ln \rho_{gas} + C \right) \right\}^{-0.5}$$

$$= z(\rho_{gas}(z)) .$$

Normalizing the gas distribution, i.e. defining $y = \frac{\rho_{gas}(z)}{\rho_{gas}(0)}$, inserting the integration constant C and using (C22) and (C24) I find :

$$z_{gas}(Y) = \sqrt{\frac{\sigma_{z,gas}^2}{8\pi G \rho_{gas}(0)}} \times \int_Y^1 \frac{dy}{y} \sqrt{\left(\frac{1}{(1 + \rho'_{s,g} p_{sg}) - (y + \rho'_{sg} p_{sg} y^{p_{gs}}) - (\rho'_{h,g} + \rho'_{r,g}) \ln(y)} \right)} . \quad (C28)$$

Notice that the term $(\rho'_{s,g} p_{sg})$ equals the ratio of stellar and gaseous kinetic energy in the midplane. For vanishing stellar, halo, and rotational densities (i.e. $\rho'_{s,g} = \rho'_{h,g} = \rho'_{r,g} = 0.0$ so that the gas is fully self-gravitating), it can be shown that (C28) then reduces to the familiar self-gravitating solution, $\rho_{gas}(z) \propto \text{sech}^2(z/z_0)$, indeed.

Investigating equation (C28), we see that there is no solution possible when the sum of the rotation and DM-halo density is negative (i.e. for a steeply rising rotation curve) because at small fractional densities, Y , the logarithmic term goes to $-\infty$ and hence dominates, leading to a negative term inside the square root. Bottema *et al.* (1987), applying the local approach, find that the rotation term can contribute significantly in the steeply rising parts of galactic rotation curves. Obviously, since galaxies do not have holes in those regions where the rotation curve rises, at least one of the assumptions must break down. Most likely, deviations from cylindrical symmetry become important and the equation of hydrostatic equilibrium is no longer a good approximation to the vertical Jeans equation.

An iterative procedure is followed to find the vertical density distribution of the gas. Starting from initial guesses for stars and gas, a solution of (C28) is calculated, which provides a new (normalized) z -distributions for the first component. Note that this equation can be inverted to calculate the vertical distribution of the stars from the z -distribution of the gas merely by interchanging the g and s indices. In order to eliminate numerical instabilities, I chose the calculated component (i.e. the LHS of [C28]) to be the component with the smallest velocity dispersion. The normalized distribution, $z_{gas}(Y)$ is then inverted to yield $\rho_{gas}(z)$ which is then scaled so that its z -integral yields the appropriate surface density. The stellar density distribution is then calculated by raising the gaseous distribution to the power p_{gs} (i.e. applying the equivalent of equation [C22]) followed by the surface density normalization. From the new midplane values the next solution of (C28) is calculated, ... until consecutive changes become small. For a given stellar velocity dispersion, the stellar vertical density distribution changes in each iteration step. In order to keep the thickness of the stellar disk fixed, as suggested by observation (vdKS81a&b; vdKS82a&b; BD93), I change the stellar velocity dispersion after each iteration step accordingly. This procedure can be easily expanded to include “N” isothermal components.

The local dark matter density can be determined in an iterative manner as well. An upper limit to the local dark matter density can be found by assuming that all other components are massless. Using the Gaussian-equivalent method (equation [14]), the measured width and velocity dispersion of the gas layer the upper limit of the dark matter density is calculated. A lower limit to the local dark matter density

is of course zero. For a values of the dark matter density halfway between the lower and upper limit, the model gas-layer thickness is calculated and compared with the observed value. If the calculated thickness corresponding to this trial DM-density value is larger than the observed value, then the lower bound is increased to the trial value. This procedure is repeated until convergence is reached. Model calculations show that beyond the optical disk, it is possible to accurately recover the input (into eqn. [C28]) DM densities from simulated thickness measurements.

D. Four Special Cases

Here I describe the gaseous distribution in the vertical direction for four interesting limiting cases with very different flaring behavior. In the first three of those, the rotation curve is assumed to be constant, while the fourth case represents gas in a region where the rotation curve is falling. In all but the self-gravitating case, the gas is treated as a massless testparticle component. The results are listed below, where all widths, $W_{gas} (\approx FWHM/2.35$, as defined by eqn. [5]), are expressed in kpc.

Fully self – gravitating gas :

$$W_{gas}^{self}(R) \approx 6.74 \left(\frac{\sigma_{10}^2}{\Sigma_1(R)} \right) \quad (D29)$$

Gas in a stellar disk :

$$W_{gas}^{stars}(R) \approx 0.08 \sqrt{\left(\frac{z_{0,400}}{\mu_{100}(0) \mathcal{M}/\mathcal{L}_2} \right)} \times \sigma_{10} \exp \frac{R}{2h_R} \quad (D30)$$

Gas in a (flattened) dark halo mass distribution :

$$W_{gas}^{halo}(R) \approx \sqrt{q \left(\frac{2.436}{1.436 + q} \right)} \times \left(\frac{\sigma_{10}}{V(\infty; 1)_{halo,100}} \right) \sqrt{R_{c,10}^2 + (R_{10}/\mathcal{C}(q))^2} \quad (D31)$$

Gas in Keplerian falloff region :

$$W_{gas}^{rot}(R) = 0.484 \frac{\sigma_{10}}{\sqrt{M_{tot,11}}} R_{10}^{\frac{3}{2}} \quad (D32)$$

where σ_{10} is the gaseous velocity dispersion in units of 10 km/s, $\Sigma_1(R)$ the gaseous surface density in units of solar masses per pc², $z_{0,400}$ the scale height of the stars in units of 400 pc, $\mu_{100}(0)$ the central surface brightness in units of 100 L_{\odot}/pc^2 , $\mathcal{M}/\mathcal{L}_2$ is the number of solar masses per solar luminosity, h_R is the radial scale length of the (exponential) stellar disk, $V(\infty; 1)_{halo,100}$ the asymptotic rotation velocity of the round dark halo in units of 100 km/s, $R_{c,10}$ the core radius of the dark halo in units of 10 kpc, R_{10} , the galactocentric radius in 10 kpc, $\mathcal{C}(q)$, is the core radius correction factor arising from the flatness, q , of the DM halo (is of order unity, see equation [A8]), and $M_{tot,11}$ the total mass of the galaxy in units of $10^{11} M_{\odot}$.

Notice that the thickness of the gas layer in a potential which is completely dominated by the rotation density is of the same order of magnitude as a gas layer in a DM-halo potential only. Such situations may arise for galaxies where the rotation curve falls in a close to Keplerian manner.

If one really wants to use the local approach (e.g. for quick estimation purposes) instead of the global approach, one might as well use the approximation to equation (C28) I found to be accurate to about 10% over a wide range of parameters. W_{gas}^{approx} can be found from :

$$\left(\frac{1}{W_{gas}^{approx}}\right)^2 = \left(\frac{w_g}{W_{gas}^{self}}\right)^2 + \left(\frac{1}{W_{gas}^{no-self}}\right)^2, \quad (D33)$$

where

$$\left(\frac{1}{W_{gas}^{no-self}}\right)^2 = \left(\frac{1}{W_{gas}^{stars}}\right)^2 + \left(\frac{w_{hr}}{W_{gas}^{halo}}\right)^2 + \left(\frac{w_{hr}}{W_{gas}^{rot}}\right)^2, \quad (D34)$$

with

$$w_g = \frac{(1.15 \Sigma_{gas} + 1.55 (\Sigma_{stars} + \Sigma_{halo} + \Sigma_{rot}))}{(\Sigma_{gas} + \Sigma_{stars} + \Sigma_{halo} + \Sigma_{rot})},$$

$$w_{hr} = \frac{(1.20 \Sigma_{stars} + 1.05 (\Sigma_{halo} + \Sigma_{rot}))}{(\Sigma_{stars} + \Sigma_{halo} + \Sigma_{rot})},$$

and

$$\Sigma_{halo} = \rho_{halo} \times W_{gas}^{no-self} \quad \text{and} \quad \Sigma_{rot} = \rho_{rot} \times W_{gas}^{no-self},$$

where the relations for the halo and rotation surface densities are evaluated (eqn. [D34]) using $w_{hr} = 1.0$. The widths, W_{gas}^i , are the widths as found for the special cases (according to the equations [D29], [D30], [D31] and [D32]). Inside the stellar disk, the width of the gas layer is mostly determined by the gas-inside-stellar-disk term, W_{gas}^{stars} . Beyond, the halo-term, W_{gas}^{halo} , dominates. The self-gravity of the gas perturbs the dominant term slightly, but with a different numerical coefficient for the two regimes because of the different form of the unperturbed z-distribution functions ($\text{sech}^{2p_{sg}}(z/z_0)$ versus Gaussian respectively).

I have tested this approximation for several cases. The first case corresponds to BE89's mass distribution for NGC 3198. The second case corresponds to a $\gamma=0.6$ -disk in a flattened ($q = 0.1$) dark halo, thereby minimizing the stellar and maximizing the dark halo contribution. The third case consists of BE89's halo and stellar mass model but with the gas surface density multiplied by a factor of ten. In the last test case I also multiply the halo densities by a factor of ten. In all these cases equation (D33) recovers the exact solution to equation (C28) to within 10 %.

REFERENCES

- Albada, T.S., van, Bahcall, J.N., Begeman, K., Sancisi, R., 1985, ApJ, 295, 305 (ABBS85)
- Albada, T.S. van, Sancisi, R., 1986, Phil. Trans. R. Soc. Lond. A., 320 447
- Athanassoula, E, Bosma A., Papaioannou, P., 1987, A&A, 179, 23 (ABP87)
- Bahcall, J.N., 1984 , ApJ, 276, 156
- Bahcall, J.N., Casertano, S., 1985, ApJ, 293, L7
- Barteldrees, A., Dettmar, R.J., 1993, A&AS, 1994, 103, 475
- Begeman, K.G., 1987, Ph. D. Thesis, Rijksuniversiteit te Groningen
- Begeman, K.G., 1989, A&A, 223, 47 (BE89)
- Blitz, L., Magnani, K., Mundy, L., 1984, ApJ, 282, L9
- Bosma, A., 1978, Ph.D. Thesis, University of Groningen
- Bottema, R, 1993, A&A, 275, 16
- Bottema, R, van der Kruit, P.C., Freeman, K.C., 1987, A&A, 178, 77
- Broeils, A.H., 1992, Ph. D. Thesis, University of Groningen
- Carignan, C., Freeman, K.C., 1988, ApJ, 323, L33
- Casertano, S., 1983, MNRAS, 203, 735
- Casertano, S., van Gorkom, J.H., 1991, AJ, 101, 1231
- Corradi, R.L., Boulesteix, J., Bosma, A., Amram, P., Capaccioli, L., 1991, A&A 244, 27
- Dekel, A, Shlosman, I, 1983, in "Internal Kinematics and Dynamics of Galaxies", IAU Symposium 100, ed. E. Athanassoula (Dordrecht, Reidel, 197)
- Dickey, J.M., Hanson, M.M, Helou, G., 1990, ApJ, 352, 522
- Efstathiou, G, Lake, G., Negroponte, J, 1982, MNRAS, 199, 1069
- Gilmore, G., Reid, N., 1983, MNRAS, 202, 1022
- Hoffner, P., Sparke, L., 1994, ApJ, 428, 466
- Van der Hulst, J.M., Terlouw, J.P., Begeman, K.G., Zwitser, W. and Roelfsema, P.R., 1992, in "Astronomical Data Analysis Software and Systems I", ed. D.M. Worall, C. Biemesderfer and J. Barnes, PASP Conf Series No. 25, p. 131
- Kamphuis, J., 1993, Chapter 12, Ph.D. Thesis Rijksuniversiteit te Groningen
- Kent, S, 1987, AJ, 93, 816
- Kruit, P.C. van der, 1981, A&A, 99, 298
- Kruit, P.C. van der, 1986, A&A, 157, 230
- Kruit, P.C. van der, 1988, A&A, 192, 117
- Kruit, P.C. van der, Searle, L., 1981a, A&A, 95, 105 (vdKS81a)
- Kruit, P.C. van der, Searle, L., 1981b, A&A, 95, 116 (vdKS81b)
- Kruit, P.C. van der, Searle, L., 1982a, A&A, 110, 61 (vdKS82a)
- Kruit, P.C. van der, Searle, L., 1982b, A&A, 110, 79 (vdKS82b)
- Kruit, P.C. van der, Shostak, G.S., 1982, A&A, 105, 351
- Kuijken, K., Gilmore, G., 1989, MNRAS, 239, 571 (KG89)

- Kundić T., Hernquist, H., Gunn, J.E., 1993, p 592 in “Back to the Galaxy”, AIP Conference proceedings # 278, Editors S.S. Holt, F. Verter
- Lake, G., Feinswog, L., 1989, AJ, 98, 166 (LF89)
- Malhotra, S., 1994, ApJ, 433, 687
- Maloney, P., 1992, p. 117, in “The Evolution of Galaxies and their Environment”, 1992, NASA conference Publication 3190, Editors D. Hollenbach, H. Thronson, J.M. Shull
- Maloney, P., 1993, ApJ, 414, 41 (M93)
- Merrifield, M.R., 1992, AJ, 103, 1552
- Olling, R., Gorkom, J.H. van, 1992, p. 374 in “The Evolution of Galaxies and their Environment”, 1992, NASA conference Publication 3190, Editors D. Hollenbach, H. Thronson, J.M. Shull
- Olling, R., Gorkom, J.H. van, 1995, in “Dark Matter”, 5th Astrophysics Conference in Maryland, AIP Conference proceedings (in press)
- Persic, M., Salucci, P., 1988, MNRAS, 243, 131
- Pfenniger, D., Combes, F., Martinet, L., 1994a, A&A, 285, 79
- Pfenniger, D., Combes, F., 1994b, A&A, 285, 94
- Press, W.H., Flannery, B.P, Teukolsky, S.A., Vetterling, W.T., 1990, in “Numerical Recipes”, Cambridge University Press
- Pritchett, C., 1983, AJ, 88, 1476
- Rubin, V.C., Ford, W.K., Thonnard, N., 1980, ApJ, 238, 471
- Rupen, M.P., 1991, Ph.D. thesis, Princeton University
- Sackett, P.D., Sparke, L.S., 1990, ApJ, 361, 408 (SS90)
- Sackett, P.D., Rix, H.W., Jarvis, B.J., Freeman, K.C., 1994, ApJ, 436, 629 (SRJF94)
- Sackett, P.D., Morrison, H.L., Harding, P., Boroson, T.A., 1994b, Nature, 370, 11 August p. 441
- Sancisi, R., Allen, R.J., 1979, A&A, 74, 73
- Sparke, L, Casertano, S, 1988, MNRAS, 234, 873
- Shostak, G.S., Kruit, P.C. van der, 1984, A&A, 132, 20
- Toomre, A, 1983, in “Internal Kinematics and Dynamics of Galaxies” , IAU Symposium 100, ed. E. Athanassoula (Dordrecht, Reidel, 177)
- Wainscoat, R.J., Freeman, K.C., Hyland, A.R., 1989, ApJ, 337, 163
- Yoshi, Y., Ishida, K., Stobie, R.S, 1987, AJ, 93, 232

Fig. 1.— The lower panel shows the rotation curves of a family of DM-halo models with varying flattening ($q = c/a = 1.0, 0.7, 0.3, 0.1$), central density ($\rho_{h,0}(q)$, equation [A9]) and core radius ($R_c(q)$, equation [A8]). The fact that all curves fall on top of each other illustrates that the equatorial rotation curve alone is not sufficient to determine the shape of the DM-halo. In the top panel I present the ratio of the rotation curve of the flattened to the round DM-halo for the same q 's as in the bottom panel. Although the residuals show systematic behavior, the amplitudes are smaller than the routinely obtained observational uncertainties (i.e. BE89)

Fig. 2.— In this figure I present the q -dependence of the DM-halo central density (top panel, equation [A9]) and core radius (lower panel, equation [A8]). With these functional forms for $\rho_{h,0}(q)$ and $R_c(q)$, the resultant equatorial DM-halo rotation curve is almost independent of q (see Figure I).

Fig. 3.— Here I show the dependence of the DM-halo parameters on the mass-to-light ratio of the stellar disk. As an example I used the parameters valid for NGC 3198 ($L(0)=207.1 L_{\odot}/\text{pc}^2$, $h_R = 2.3$ kpc, $z_e = 0.23$ kpc). The gaseous surface density distribution and rotation curve ($V_{obs}(2.3h_R) = 145.8$) were taken from BE89, who used Kent’s (1987) photometry to calculate the rotation curve due to the stellar disk ($f_m = 0.899$ and $f_{10} = 0.578$). In the lower right panel the \mathcal{M}/\mathcal{L} -ratio is presented as a function of γ (defined by eqn. [B15]). In the upper left and lower left panel I show the DM-halo central density, $\rho_{h,0}$, and its core radius, R_c respectively. The dark-to-stellar mass ratio is presented in the upper right panel. To indicate the sensitivity of the halo parameters on the slope of the rotation curve, I calculated them for three values : the appropriate β_8 -value for NGC 3198 (0.985) and the $\pm 5\%$ values.

Fig. 4.— In this figure I present fits to the rotation curve of NGC3198 with different γ values. In the lower panel I present the observed rotation curve (open squared), the rotation curve due to the HI-disk (crosses) and several disk-halo combinations [full line, gas+($\gamma=0.9$ -stellar-disk)+DMhalo, $\mathcal{M}/\mathcal{L} = 2.96, \rho_{h,0} = 11.2, R_c = 6.26$; dotted line, gas+($\gamma=0.7$ -stellar-disk)+DMhalo, $\mathcal{M}/\mathcal{L} = 1.79, \rho_{h,0} = 92.6, R_c = 2.00$; dashed line, gas+($\gamma=0.5$ -stellar-disk)+DMhalo, $\mathcal{M}/\mathcal{L} = 0.92, \rho_{h,0} = 684, R_c = 0.73$], where the central densities are expressed in units of mM_{\odot}/pc^3 and the core radii in units of kpc. The upper panel shows the velocity difference between observations and model. The large $\gamma = 0.9$ -value corresponds to the “maximum-disk” solution. A better fit is the $\gamma = 0.5$ -solution (low \mathcal{M}/\mathcal{L} -disk) close to the value proposed by Bottema (1993). Furthermore, since the velocity field of the inner parts of NGC 3198 deviates from axisymmetric rotation (Corradi *et al.* , 1991), the discrepancies between observed and model curves in the inner regions seem irrelevant. The only free parameter in the fitting procedure I used (described in Appendix B) is γ (defined by eqn. [B15]). The observed rotation curve (and the errors, i.e. the difference between both sides, are indicated by the error bars), the rotation curve due to the gaseous disk, the rotation curve due to the stellar disk and the optical parameters were taken from BE89.

Fig. 5.— For a model galaxy (consistent with the parameters of NGC 3198 as observed by BE89) we compare the midplane mass densities inferred from the thickness of the gas layer (ρ_{INF} , using the local approach via equation [14], where $\sigma_{(z,gas)}=7.5$ km/s) with the true stellar midplane densities ($\rho(\text{STARS})_{INP}$, left-hand set of panels), the true (stellar+DM-halo) densities ($\rho(\text{STARS} + \text{HALO})_{INP}$, middle set of panels), and the true (stellar+DM-halo+rotation) densities ($\rho(\text{STARS} + \text{HALO} + \text{ROT})_{INP}$, right-hand set of panels). The truncation of the stellar disk at $6h_R$ is easily recognized for almost all disk-halo models. The self-gravity of the gas has not been included in these calculations. The bottom two panels were calculated for a round halo, while the top panels corresponds to a flattened ($q = 0.1$) DM-halo. The lines correspond to models with different γ values (full line : $\gamma = 0.9$, dotted line : $\gamma = 0.8$, short dashed line : $\gamma = 0.7$ and the long dashed line : $\gamma = 0.6$). For most models, the ratio of derived-to-input densities (vertical axis) deviates significantly and systematically from unity so that the Gaussian-equivalent method can not be used to reliably determine the midplane volume densities (see also §3.1.)

Fig. 6.— In this collage of model galaxies, each plot represents the vertical force, $K_z(z; \gamma, q)$, as a function of height above the plane (z). The top plots correspond to a $\gamma=0.9$ -disk, the lower two plots to a $\gamma=0.6$ -disk. The left-hand side plots were calculated for a round ($q = 1.0$) halos; the two right most plots for a flat ($q = 0.1$) halos. The different panels inside each plot correspond to different radii (in units of h_R). All panels have been calculated for a galaxy model consistent with the observed properties of NGC 3198 (BE89). The open squares represent the vertical force due to a double exponential stellar disk. The dashed line is the vertical force valid for the local approximation. The full line is the sum of the vertical force from the stellar disk and DM-halo. We notice that the maximum-disk plus round DM-halo combination is the only region in γ, q -space where the stellar disk is dominant over the entire extent of the stellar disk ($R \lesssim 5h_R$). For this combination of γ and q , the stellar disk contributes significantly ($\approx 20\%$ at $11 h_R$) to the vertical force, even beyond the truncation of the stellar disk (at $6h_R$). Furthermore notice, that the *shapes* of the vertical forces generated by a very flattened DM-halo are very similar to the *shapes* of the vertical force in a round DM-halo, but that the *amplitudes* are about twice larger.

Fig. 7.— This figure presents the vertical force in the region beyond the optical disk. Again, the galaxy model used, stars+DM-halo+gas, is consistent with the observed properties of NGC 3198 (BE89). The full line is the sum of the vertical force due to the stellar disk, the DM-halo and the gas layer. The dotted lines represent the $K_z(z)$ due to the flattened DM-halo only ($q = 1.0$ and 0.3 for the Figures 7a (left-hand plot) and 7b (plot on the right-hand side) respectively). The vertical force arising due to the (truncated) stellar disk is represented by the short dashed line. The long dashed line represents the self-gravity of the gas, which' contribution to the total vertical force can be rather important (30-40%) beyond the optical disk.

Fig. 8.— In this figure I illustrate the dependence of the thickness of the gas-layer, $W_{gas} (\approx FWHM/2.35$, as defined by eqn. [5]), upon its self-gravity. I used the multi-component approximation discussed in Appendix C to calculate NGC 3198-like mass models with varying amounts of gas. For the mass models with the differently scaled gaseous surface densities I performed a separate disk-halo decomposition, all yielding similarly acceptable fits to the observed rotation curve. The left-hand set of panels shows (for $q = 0.1$, $q = 0.5$, and $q = 1$ from top to bottom) the flaring of the gas-layer for several gas-surface-density scaling factors. The scale factor, s , is defined such that $\Sigma_{gas,Model} = s\Sigma_{gas,observed}$; full line, $s = 0.01$; dotted line, $s = 1$; short dashed line, $s = 5$; long dashed line, $s = 10$. In the right-hand set of panels I plot the thickness ratio of scaled surface density to the zero surface density case. From these plots it is clear that the effects of the self-gravity are moderate, but vary systematically with radius for the observed gaseous surface densities. For the upwardly scaled surface densities I find almost no dependence of the gas-layer width on the halo flattening.

Fig. 9.— In the bottom panel I compare the thickness of the gas layer ($W_{gas} (\approx FWHM/2.35$, as defined by eqn. [5])) as calculated in the global approach (the lines with the filled circles) with the thickness as calculated from the multi-component approach (the lines). For both approaches a fixed $\text{sech}^2(z/(2z_e))$ stellar distribution, truncated at $R/h_R=6$, was used. Three different DM-halo flattenings are shown (from top to bottom: $q = 1.0$, full line; $q = 0.3$, dashed line; $q = 0.1$, dotted line). In the top panel I plot the percentage difference between the two approaches. The difference between the global and multi-component method mainly arises due to small scale structure in the observed rotation curve, which has been used to calculate ρ_{rot} .

Fig. 10.— For a given rotation curve (BE89), I show how the thickness of the gas layer ($W_{gas}(\approx FWHM/2.35$, as defined by eqn. [5])) depends on the flattening of the DM-halo ($q = c/a$). The different line-types/symbols correspond to different halo flattenings q ; $q = 1.0$ (full line), $q = 0.8$ (dotted line), $q = 0.6$ (short dashed line), $q = 0.3$ (long dashed line)), and $q = 0.1$ (filled circles). The model curves presented were calculated for a gaseous velocity dispersion of 7.5 km/s. The left-hand side figure was calculated using a double exponential stellar disk, which is replaced by a truncated stellar disk for the middle panel. For the right-hand side plot I included the truncation of the stellar disk as well as the self-gravity of the gas. For these particular mass models the gaseous self-gravity influences the model widths more strongly than the truncation of the stellar disk does.

Fig. 11.— This figure shows how the thickness of the gas layer ($W_{gas}(\approx FWHM/2.35$, as defined by eqn. [5])) depends on the mass-to-light ratio of the stellar disk for several galaxy models (truncated-stellar-disk+*round*-DM-halo) consistent with the observed properties of NGC 3198 (BE89). The different line types correspond to different mass-to-light ratios of the stellar disk ; ($\mathcal{M}/\mathcal{L} = 2.98$, $\gamma = 0.9$) full line, ($\mathcal{M}/\mathcal{L} = 2.35$, $\gamma = 0.8$) dotted line, ($\mathcal{M}/\mathcal{L} = 1.80$, $\gamma = 0.7$) short dashed line, ($\mathcal{M}/\mathcal{L} = 1.32$, $\gamma = 0.6$) long dashed line. Inside the optical disk, the extreme thinness of the HI disk (in absolute measures) will, quite likely, limit its usefulness for the determination of the \mathcal{M}/\mathcal{L} -ratio of the stellar disk to the nearest galaxies. Beyond the optical disk, the thickness of the gas layer becomes virtually independent of the mass-to-light-ratio of the stellar disk, so that a determination of the DM-halo flattening is independent of \mathcal{M}/\mathcal{L} . As for Figure 10 the model curves presented were calculated for a gaseous velocity dispersion of 7.5 km/s.

Fig. 12.— This figure illustrates one of the observable effects of a flaring HI-layer. The apparent gaseous velocity dispersion (i.e. the second moment w.r.t. recession velocity) of two galaxy models is shown here (the *input* dispersion was 7.5 km/s). The upper panel was calculated setting the *FWHM* of the gas layer to 100 pc everywhere, while the lower panel corresponds to a model run where the vertical distribution of the HI layer was calculated in a self-consistent manner (cf. the procedure outlined in Appendix C for a model with $q = 1$). A flaring disk imprints a clearly different pattern on the apparent velocity dispersion map. Since this is a large-scale pattern, its detection should be relatively easy. The model calculations were convolved to a $15'' \times 15''$ beam, whereas the channels are square and 2.56 km/s wide. For both models I used the rotation curve and HI surface density distribution of NGC 3198 (BE89).

Fig. 13.— This figure shows that the effects of a flaring HI layer are also visible in individual channel maps. The top panel shows a channel map ($|V_{sys} - V_{chan}| = 104$ km/s, smoothed down to $30'' \times 30''$) for the thin hydrogen disk described in Figure 12. In the middle panel I show the same channel but now for the flaring-disk model. The “butterfly-wing” for the thin hydrogen layer model (upper panel) is clearly narrower and more peaked than its flaring equivalent (middle panel). Because the difference between the two models (lower panel) is significant over a large range in radii, it is expected that local irregularities (in the velocity field and/or the surface density distribution) will not be a limitation in determining the thickness of the hydrogen layer of inclined galaxies.

Fig. 14.— In this figure I present the radial dependence of the ratio of stellar to dark matter midplane density for several γ values (full line $\gamma = 0.9$, dotted line $\gamma = 0.8$, short dashed line $\gamma = 0.7$, long dashed line $\gamma = 0.6$, dash-dotted line $\gamma = 0.5$). The left most figure corresponds to a round DM-halo ($q=1.0$), the right most to a very flattened DM-halo ($q=0.1$) and the figure in the middle was calculated for a DM-halo of intermediate flattening ($q=0.4$). This ratio is calculated using the disk-halo decomposition for a flat rotation curve presented in Appendix B ([B20]). It can be clearly seen that in maximum-disk like models the stellar density dominates the midplane mass density out to about four radial scale-lengths, beyond which the contribution of the stellar density decreases sharply. For the low γ -models, the stellar density never really dominates.

Table 1.

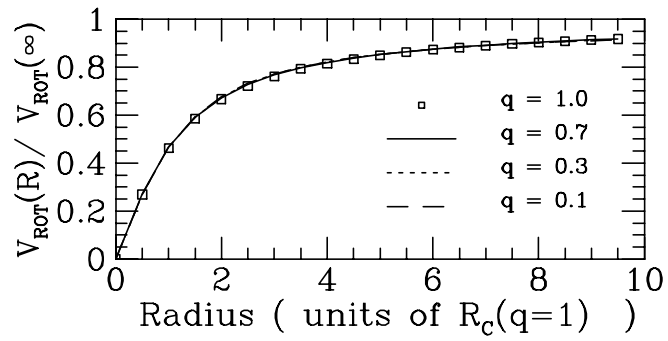
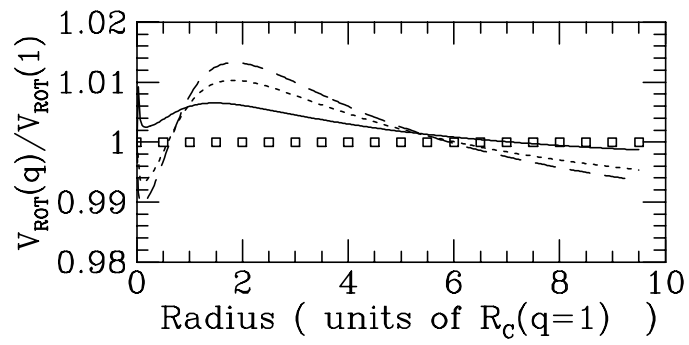
$\frac{R_{max}}{h_R}$	$z_e/h_R = 0.05$				$z_e/h_R = 0.10$				$z_e/h_R = 0.15$			
	f_m	f_6	f_8	f_{10}	f_m	f_6	f_8	f_{10}	f_m	f_6	f_8	f_{10}
2.0	0.807	0.516	0.443	0.395	0.798	0.518	0.445	0.397	0.767	0.528	0.454	0.405
2.5	0.841	0.553	0.473	0.421	0.809	0.563	0.482	0.429	0.778	0.574	0.492	0.438
3.0	0.774	0.612	0.522	0.464	0.748	0.623	0.531	0.472	0.722	0.633	0.540	0.480
3.5	0.756	0.647	0.549	0.487	0.731	0.658	0.559	0.496	0.706	0.668	0.568	0.504
4.0	0.750	0.670	0.567	0.502	0.724	0.682	0.576	0.511	0.700	0.693	0.586	0.519
4.5	0.747	0.688	0.578	0.511	0.722	0.700	0.588	0.520	0.697	0.711	0.598	0.529
5.0	0.746	0.703	0.587	0.518	0.720	0.714	0.597	0.527	0.696	0.726	0.607	0.536
5.5	0.746	0.718	0.592	0.522	0.720	0.729	0.603	0.532	0.695	0.740	0.613	0.541
6.0	0.745	0.734	0.597	0.525	0.720	0.743	0.607	0.535	0.695	0.753	0.617	0.544
6.5	0.745	0.724	0.600	0.528	0.719	0.735	0.611	0.537	0.695	0.745	0.621	0.546
7.0	0.745	0.722	0.603	0.529	0.719	0.733	0.614	0.538	0.695	0.743	0.624	0.548
∞	0.745	0.721	0.607	0.534	0.719	0.732	0.617	0.543	0.695	0.742	0.627	0.552

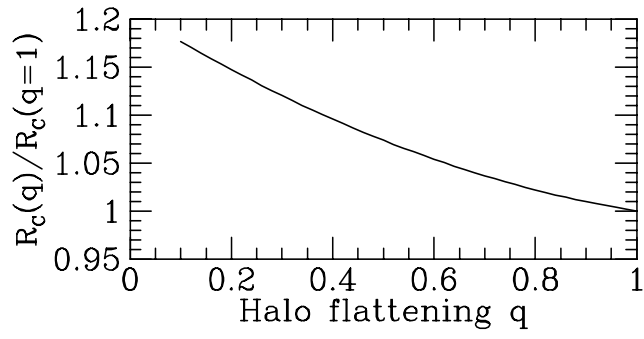
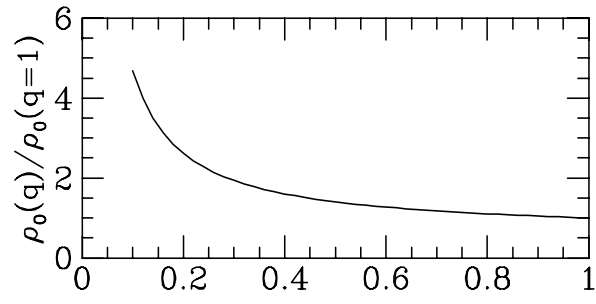
Table 1. (continued)

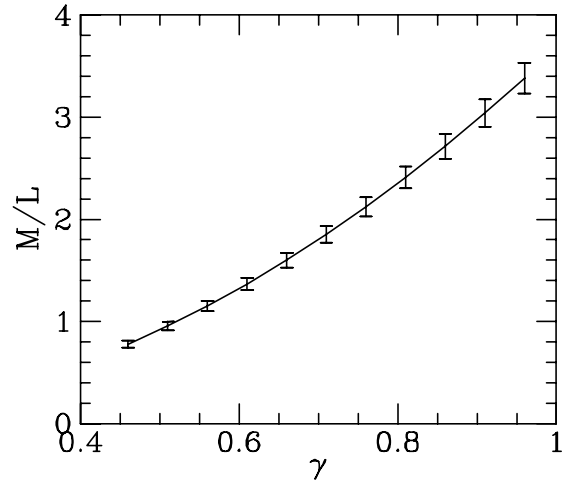
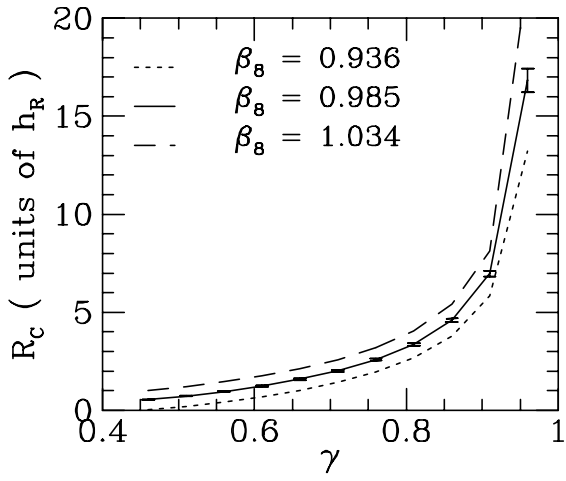
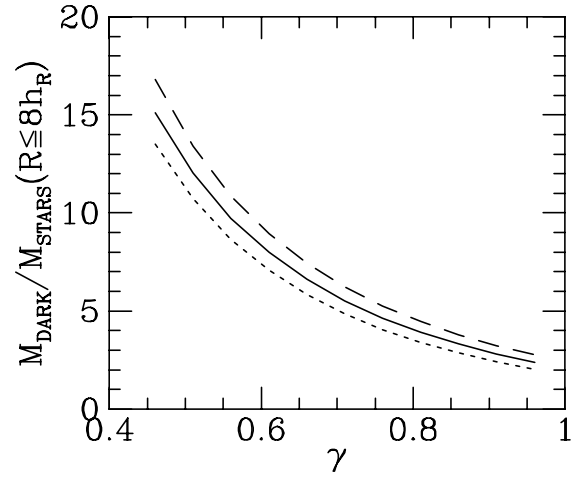
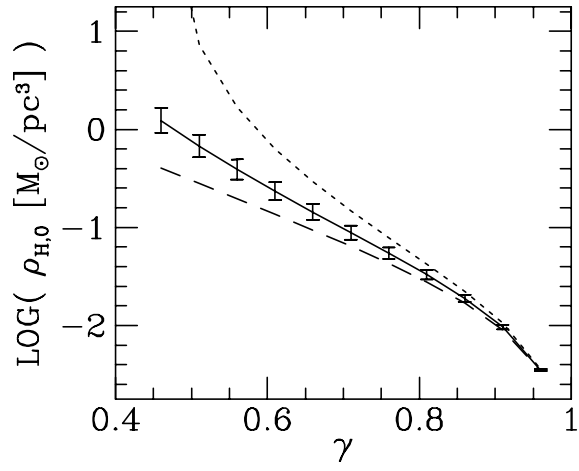
$\frac{R_{max}}{h_R}$	$z_e/h_R = 0.20$				$z_e/h_R = averaged$			
	f_m	f_6	f_8	f_{10}	f_m	f_6	f_8	f_{10}
2.0	0.748	0.534	0.460	0.410	0.780	0.524	0.451	0.402
2.5	0.749	0.584	0.501	0.446	0.794	0.569	0.487	0.434
3.0	0.698	0.643	0.549	0.488	0.736	0.628	0.536	0.476
3.5	0.683	0.679	0.577	0.513	0.719	0.663	0.563	0.450
4.0	0.677	0.703	0.596	0.528	0.713	0.687	0.581	0.515
4.5	0.674	0.722	0.608	0.538	0.710	0.705	0.593	0.525
5.0	0.673	0.737	0.617	0.545	0.709	0.720	0.602	0.532
5.5	0.672	0.751	0.623	0.550	0.708	0.735	0.608	0.536
6.0	0.672	0.762	0.628	0.553	0.708	0.748	0.612	0.539
6.5	0.672	0.755	0.631	0.555	0.708	0.740	0.616	0.542
7.0	0.672	0.754	0.634	0.557	0.708	0.736	0.619	0.543
∞	0.672	0.752	0.637	0.561	0.708	0.737	0.622	0.548

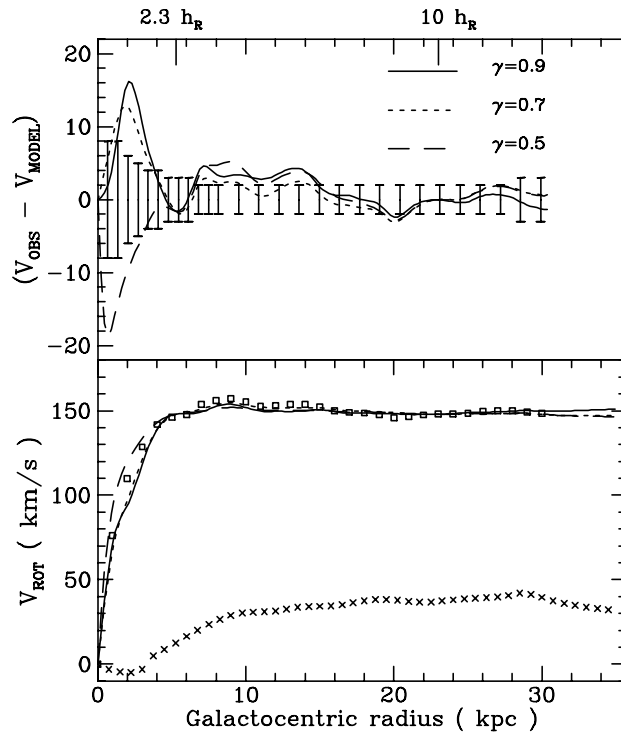
Table 2.

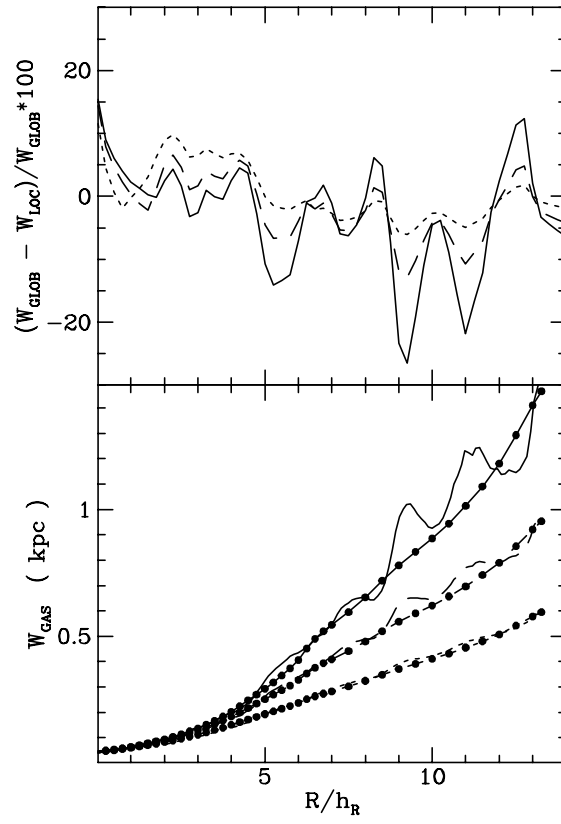
lhs-range of (B17)	$a_{6,0}$	$a_{6,1}$	$a_{6,2}$	R_c/h_R -range
$\in (1.00, 1.90]$	1.000	0.4300	0.1140	$\in (0, 1.5]$
$\in (1.90, 3.04]$	0.7363	0.7734	-0.001442	$\in (1.5, 3]$
$\in (3.04, 4.76]$	0.2709	1.097	-0.05814	$\in (3, 6]$
$\in (4.76, 5.81]$	1.400	0.7439	-0.03038	$\in (6, 10]$
lhs-range of (B17)	$a_{8,0}$	$a_{8,1}$	$a_{8,2}$	R_c/h_R -range
$\in (1.00, 2.10]$	1.000	0.4884	0.1645	$\in (0, 1.5]$
$\in (2.10, 3.71]$	0.7252	0.8293	0.05622	$\in (1.5, 3]$
$\in (3.71, 6.76]$	-0.3281	1.506	-0.05400	$\in (3, 6]$
$\in (6.76, 9.16]$	-0.01879	1.4511	-0.05341	$\in (6, 10]$
lhs-range of (B17)	$a_{10,0}$	$a_{10,1}$	$a_{10,2}$	R_c/h_R -range
$\in (1.00, 2.23]$	1.000	0.5209	0.2007	$\in (0, 1.5]$
$\in (2.23, 4.20]$	0.7508	0.8190	0.1103	$\in (1.5, 3]$
$\in (4.20, 8.47]$	-0.6623	1.702	-0.02960	$\in (3, 6]$
$\in (8.47, 12.55]$	-1.696	2.100	-0.06758	$\in (6, 10]$

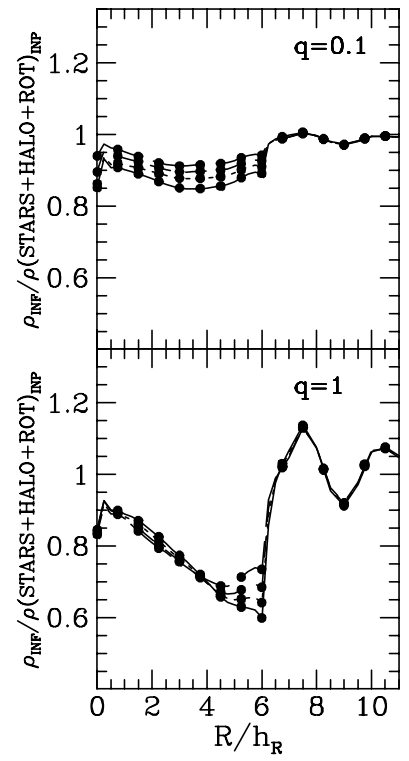
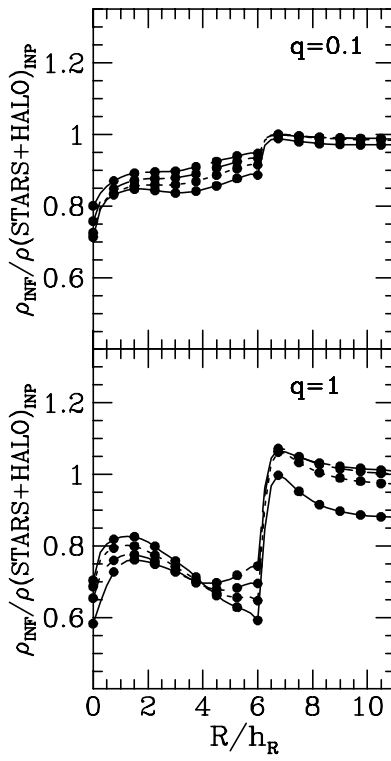
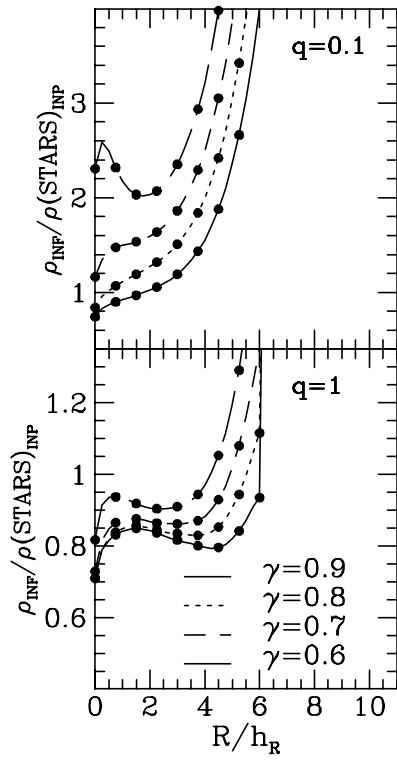


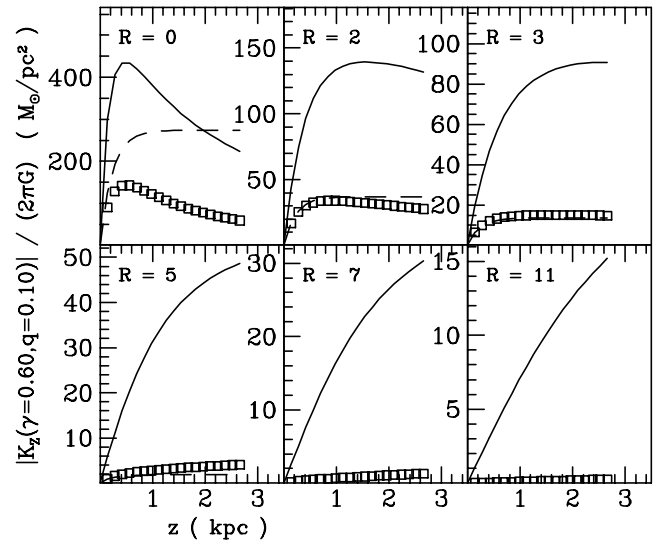
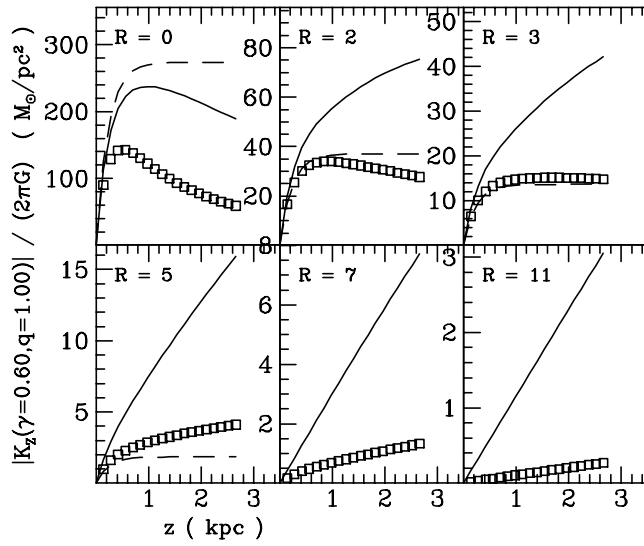
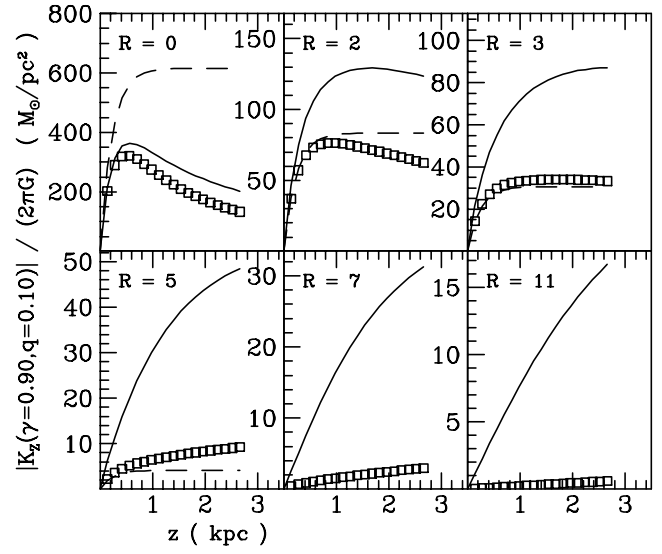
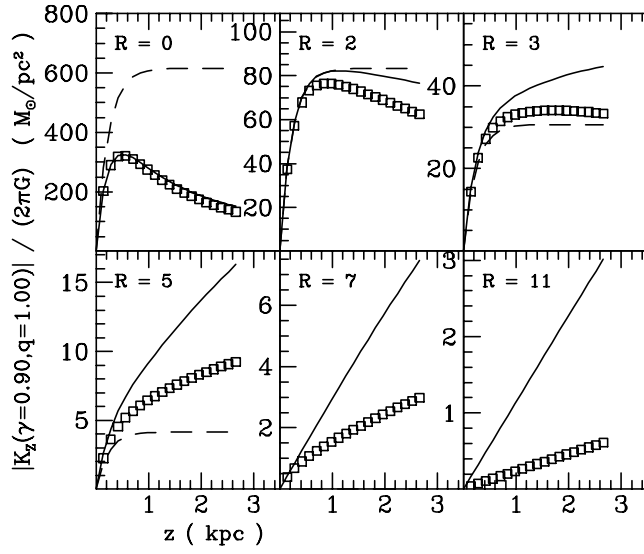


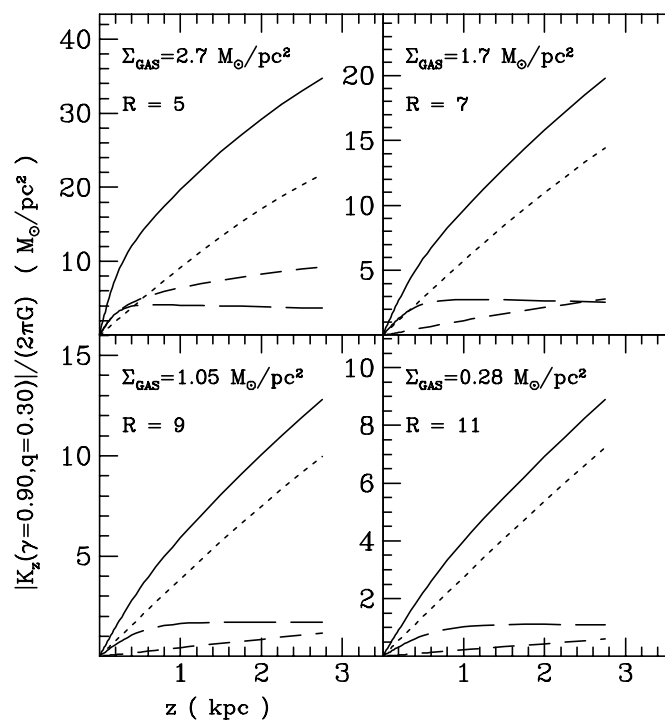
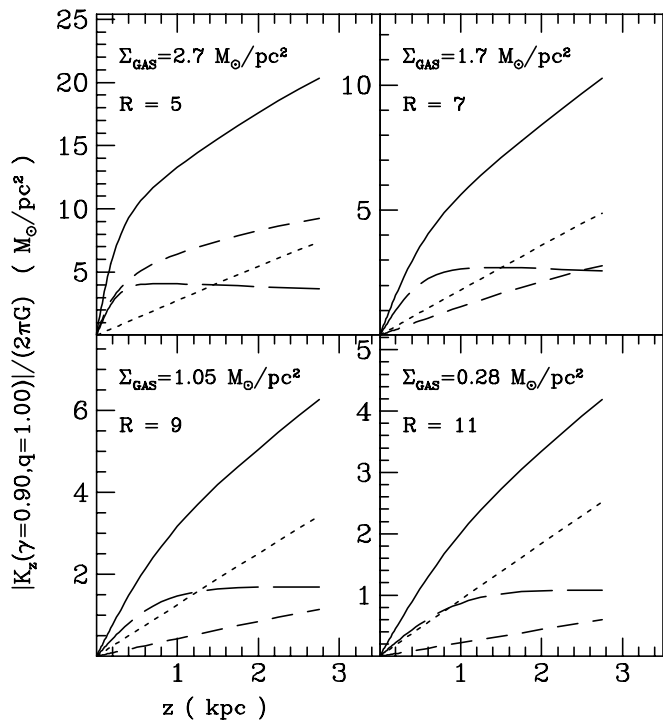


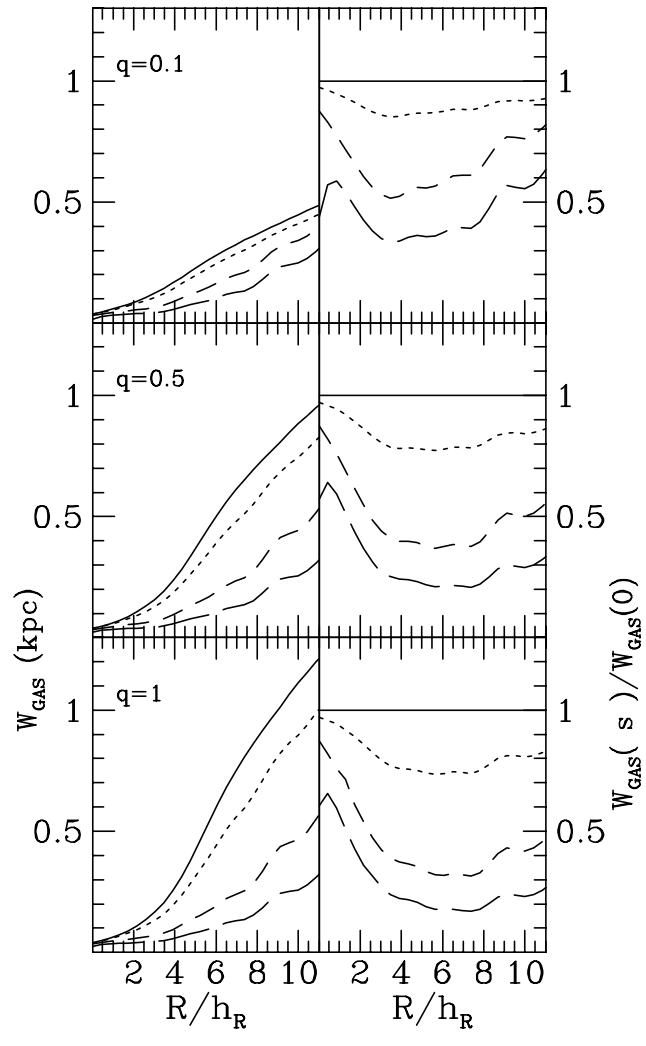


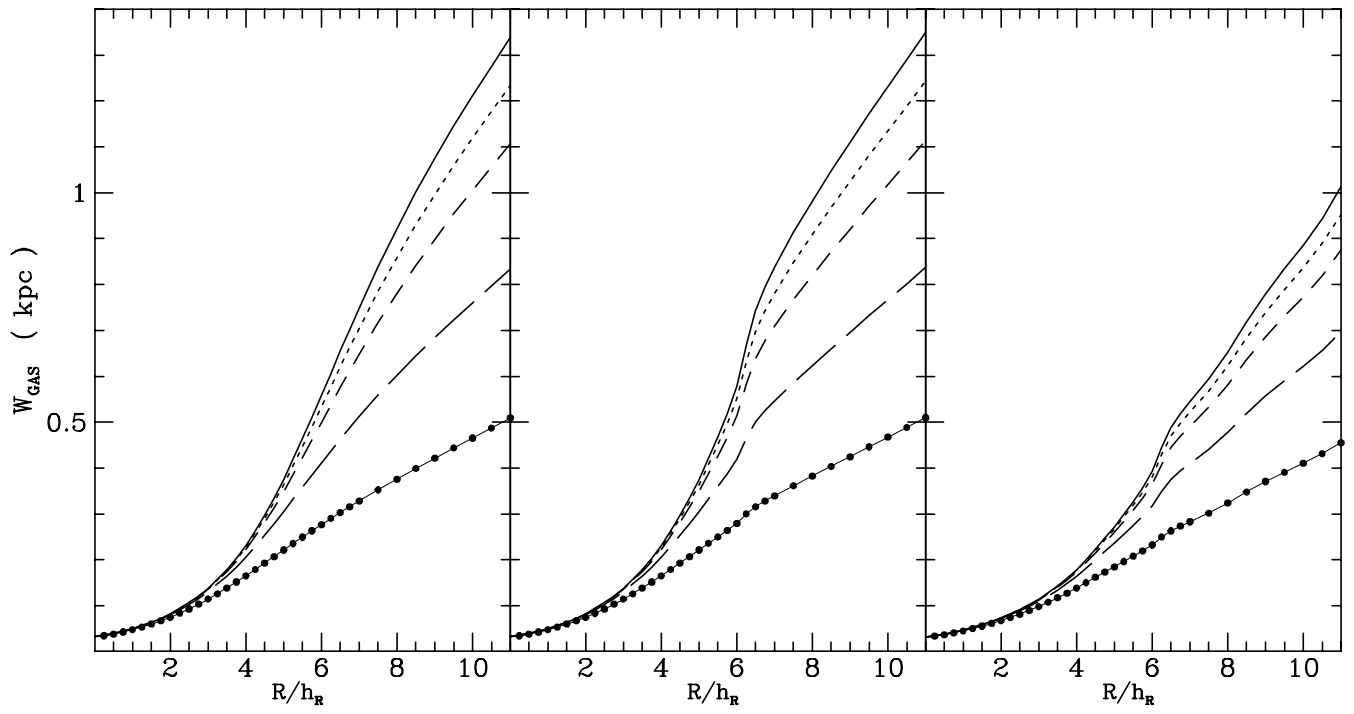


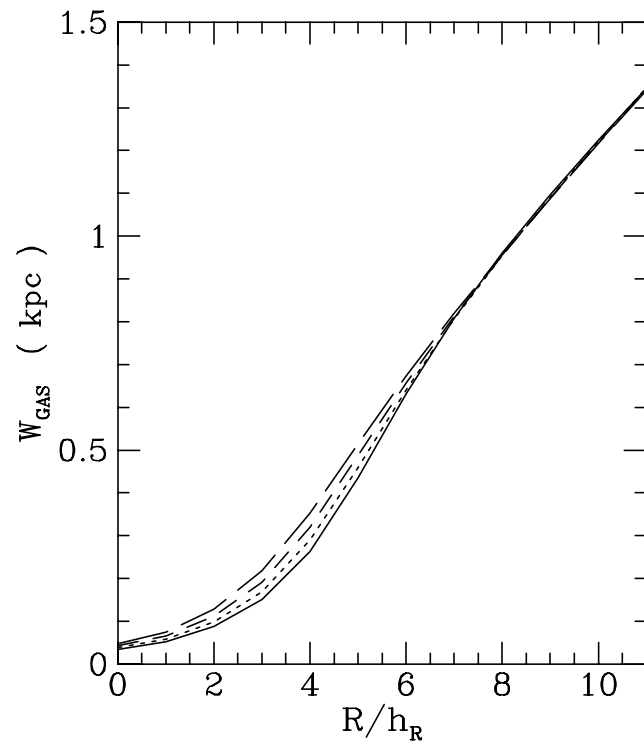






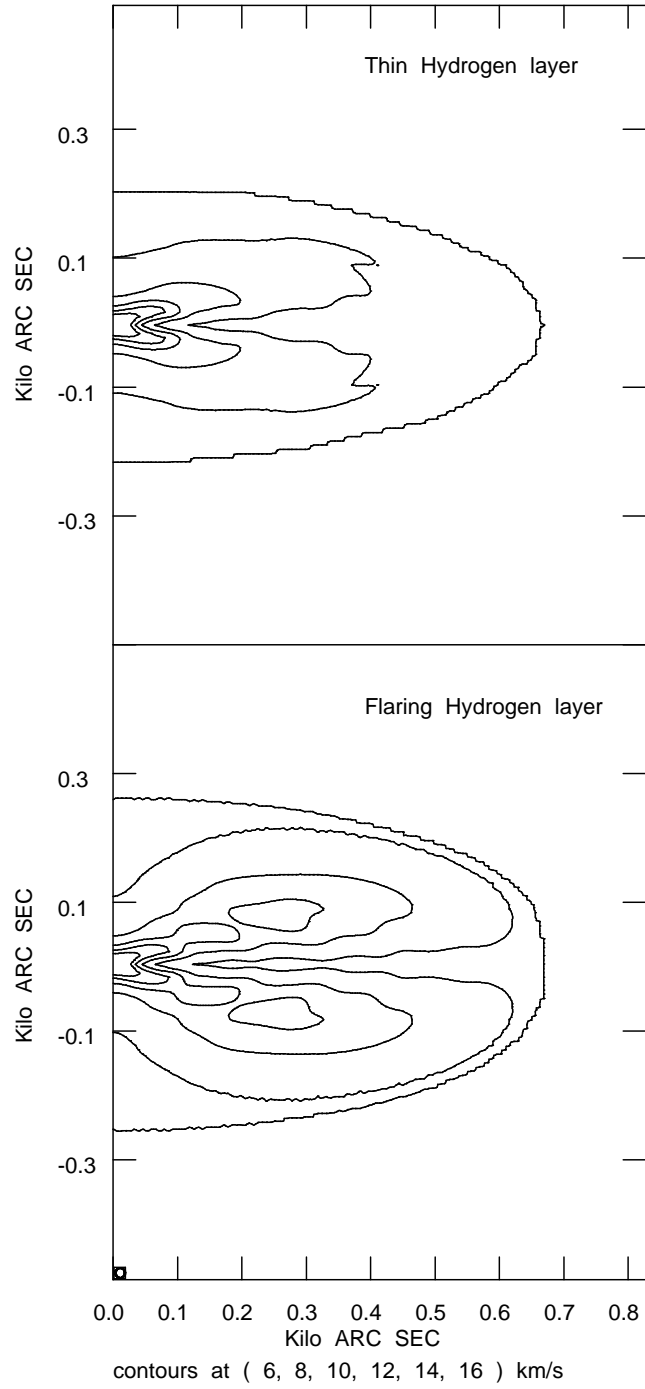




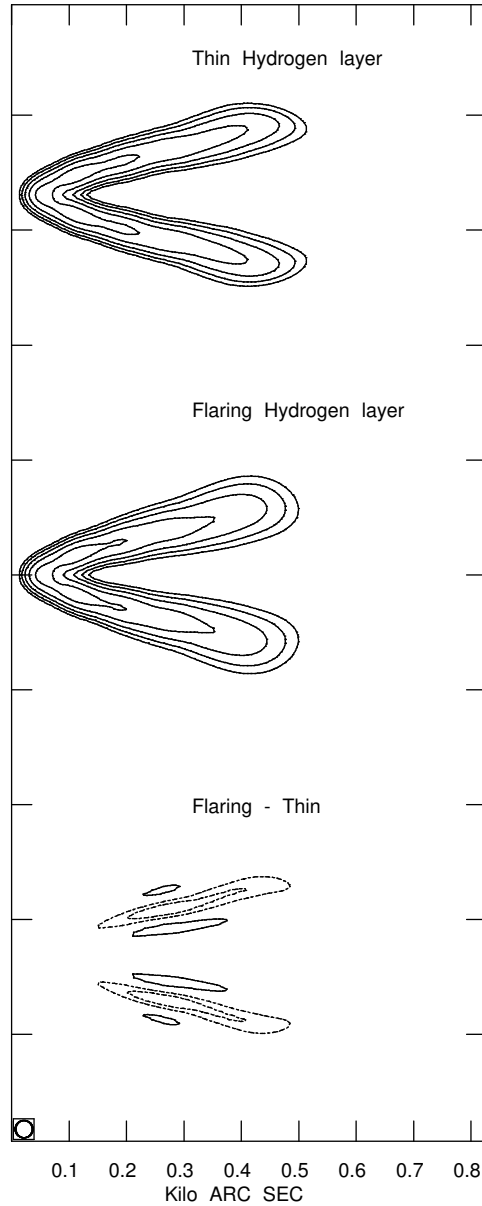


NGC 3198 models

Velocity dispersion maps for simulated galaxies



NGC 3198 models



Contours : (-3,-1.5,1.5,3,6,12,24) mJy/Beam

